A thin-film extensional flow model for biofilm expansion by sliding motility

Alexander Tam*[1], J. Edward F. Green[1], Sanjeeva Balasuriya[1], Ee Lin Tek[2], Jennifer M. Gardner[2], Joanna F. Sundstrom[2], Vladimir Jiranek[2], and Benjamin J. Binder[1]

[1]School of Mathematical Sciences, University of Adelaide, Adelaide, SA 5005, Australia.
[2]Department of Wine and Food Science, Waite Campus, University of Adelaide, Urrbrae, SA 5064, Australia.

March 22, 2019

Abstract

In the presence of glycoproteins, bacterial and yeast biofilms are hypothesised to expand by sliding motility. This involves a sheet of cells spreading as a unit, facilitated by cell proliferation and weak adhesion to the substratum. In this paper, we derive an extensional flow model for biofilm expansion by sliding motility to test this hypothesis. We treat the biofilm two-phase (living cells and an extracellular matrix) viscous fluid mixture, and model nutrient depletion and uptake from the substratum. We simplify the governing equations using a thin-film approximation, which reduces the model to axisymmetric form. After estimating parameters from mat formation experiments of *Saccharomyces cerevisiae*, we obtain good agreement between numerical solutions to our model and the experimental expansion speed. We then demonstrate how cell proliferation and death rates, fluid production rate, and movement and consumption of nutrients affect expansion speed, enabling us to predict biofilm expansion for different microbes and experimental conditions. Finally, we show that sliding motility alone can explain the ridge formation observed in some biofilms. Introducing surface tension inhibits ridge formation, by reducing transport of fluids and nutrients towards the proliferating rim. Overall, these results confirm that sliding motility is a possible mechanism for yeast biofilm expansion.

Keywords: Saccharomyces cerevisiae, yeast, mat formation experiments, lubrication theory, multi-phase flow, viscous flow

1 Introduction

Micro-organisms can form colonies with fascinating and complex spatiotemporal patterns. As these colonies are readily grown in experiments, bacteria and fungi are often used as

*Corresponding author: alexander.tam@adelaide.edu.au

model organisms to investigate the mechanisms of pattern formation in large collections of cells. Identifying the contributions of different candidate mechanisms to the self-organisation process is an important problem in developmental biology [1]. For example, Turing [2] and Keller and Segel [3] famously showed that heterogeneous patterns can develop from a homogeneous initial state as a result of reaction and diffusion of chemicals. Murray [1] proposed a more general mechanochemical theory, where chemical signals combine with mechanical interactions between cells and their environment to give rise to spatial patterns. As these mechanisms can interact in a complex manner, pattern formation in micro-organisms continues to be an active field of research.

Reynolds and Fink [4] showed that the bakers' yeast *Saccharomyces cerevisiae* can form mats when grown on semi-solid agar. These mats consist of cells embedded in a self-produced extracellular matrix (ECM), and consequently established *S. cerevisiae* as a useful model organism for fungal biofilm formation. We previously showed that a minimal reaction–diffusion model for nutrient-limited growth alone could reproduce the floral pattern observed in mat formation experiments [5]. However, experimental observations also led Reynolds and Fink [4] to hypothesise that yeast biofilms expand by sliding motility. This is a form of passive translocation, in which a sheet of cells spreads as a unit due to the expansive forces of cell growth [6], and reduced friction between the cells and substratum [7]. This mechanism was not considered in previous models.

In this work, we use a combination of mathematical modelling and experiments to investigate the extent to which sliding motility contributes to yeast biofilm formation. In §1.1 and §1.2, we review the existing literature on yeast biofilms and the mathematical modelling thereof. In §2, we derive a two-phase (living cells and the ECM) mathematical model for biofilm expansion. We then exploit the thin biofilm geometry to obtain a one-dimensional, radially symmetric thin-film approximation to the general model in §3. We compute numerical solutions to the model in §4, and show that the model can reproduce the expansion speed observed in experiments. We confirm that cell proliferation drives expansion in sliding motility, and demonstrate how movement, uptake, and consumption of nutrients affect expansion speed. We close the paper in §5, concluding that sliding motility is a plausible mechanism for biofilm formation in yeast.

1.1 Biological background

A biofilm is a slimy community of micro-organisms existing on a surface, in which cells adhere to each other and reside within a self-produced extracellular matrix (ECM). An estimated 80% of bacteria in nature exists in biofilm colonies [8]. For this reason, they have been described as the 'oldest, most successful and widespread form of life on Earth' [9], and have attracted significant research attention. Our main objective is to better understand

the mechanisms of yeast biofilm expansion. Yeasts are single-cell fungal organisms that have well-known everyday uses, for example in baking and brewing. However, yeast species such as the pathogenic *Candida albicans*, often form biofilms on indwelling medical devices [10]. These biofilms are a leading cause of infections in clinical settings, and can be up to 2000 times more resistant to anti-fungal agents than planktonic cells [8]. Inability to remove fungal biofilms can lead to candidiasis, which is an invasive disease estimated to affect around 0.2% of the population per year. Due to its high resistance to treatment, candidiasis has a mortality rate of 30%–40% in immunocompromised people [11]. However, despite these significant impacts on human health, fungal biofilms are much less widely studied than bacterial biofilms [12].

The extracellular matrix is a distinguishing feature of biofilms. It consists of water, which forms up to 97% of matrix material [13], and various extracellular polymeric substances (EPS). Although the composition and function of the ECM may differ between species, it provides biofilm colonies with several advantages over planktonic cells, as summarised by Flemming and Wingender [9]. For yeast biofilms specifically, the ECM has been observed to assist the transportation of nutrients and water [14], and prevent penetration of harmful external substances [15]. The ECM also influences biofilm rheology. Although biofilms are viscoelastic in general, on time scales longer than the order of minutes they tend to behave as viscous fluids [9, 16, 17].

The budding yeast *Saccharomyces cerevisiae* has emerged as a useful model for fungal biofilm growth in cell biology research [4]. A major advantage of using *S. cerevisiae* in experiments is that its genome has been sequenced [18], and a wide variety of genetic tools such as mutant libraries are available. As it is closely related to *C. albicans* [19], it has assumed an important role in the identification of new targets for anti-fungal therapy [4, 20]. Furthermore, as a eukaryotic organism its basic cellular processes also have a lot in common with human cells [20]. Due to this, *S. cerevisiae* has also been used as a model for understanding the division of cancer cells [12].

Reynolds and Fink [4] were the first to perform mat formation experiments with *S. cerevisiae*, and similar methods have been used in subsequent studies [5, 12, 21]. In these experiments, yeast cells are inoculated on semi-solid (0.3%) agar plates. They initially form a thin round biofilm, which over time expands and forms a complex mat structure, characterised by petal-like features at its edge. This transition is illustrated in Figure 1.1.

A notable finding of Reynolds and Fink [4] is that the glycoprotein Flo11p is required for mat formation. Similar glycopeptidolipids are prerequisites for biofilm formation in *Mycobacterium smegmatis*, as they increase cell surface hydrophobicity, which results in weak adhesion between the biofilm and substratum [7]. This led Reynolds and Fink to hypothesise that sliding motility was the driving mechanism of yeast biofilm formation.

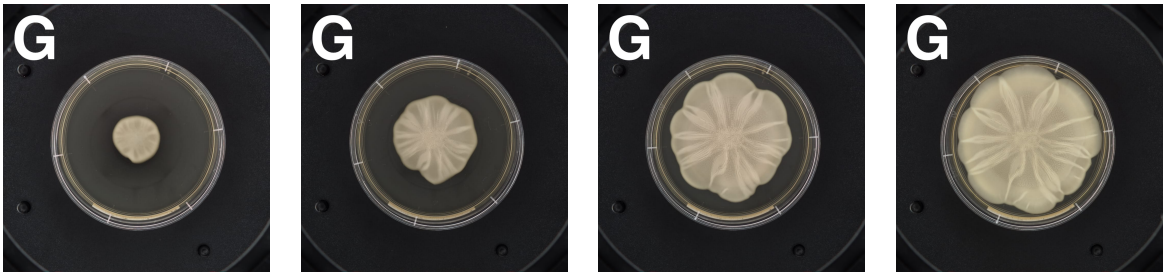

(a) 68 h. (b) 117 h. (c) 164 h. (d) 237 h.

Figure 1.1: A time series of images for a *S. cerevisiae* mat formation experiment [5].

Recent studies on bacterial biofilms have also revealed that osmotic swelling is another potential mechanism for biofilm expansion [22, 23]. This requires production of EPS, which creates an osmotic pressure difference between the biofilm and environment. The biofilm then physically expands by taking up water from the agar [22]. The extent to which sliding motility and osmotic swelling contribute to expansion depends on the microbial species and environment [23]. For example, in some bacterial biofilms including *Bacillus subtilis*, in which ECM fraction is commonly 50–90% [24] and can be as high as 95–98% [13, 25], osmotic swelling is the primary mechanism [22]. In contrast, we observe that ECM fraction is approximately 10% in *S. cerevisiae* mats, suggesting that cell proliferation and sliding motility will play a larger role. However, no detailed study into whether sliding motility is the mechanism of yeast biofilm expansion has been performed. Investigating this is the subject of our paper.

1.2 Previous models of biofilm formation

Owing to their ubiquity and importance to infections, biofilms have attracted significant attention in the applied mathematics community. Previous models have incorporated a wide variety of approaches (see Mattei et al. [24] for a comprehensive recent review). These include agent-based or hybrid models [26–28], and reaction–diffusion system [5, 12, 29–31], both of which model the spread of cells, and movement and consumption of nutrients. However, a limitation of both of these approaches is that it is difficult to include the effect of colony mechanics, such as extracellular fluid flow [32]. As modelling sliding motility requires considering the ECM mechanics, we restrict our attention here to models that incorporate the extracellular fluid.

In the literature, many models that incorporate the flow of external fluid involve biofilms growing vertically on non-reactive, impermeable substrata [33–35]. Several models also consider mechanical effects in spreading biofilms [36–38]. We focus primarily on another promising approach, which is to model the biofilm as a multi-phase mixture of fluids. In these models, biofilms are typically modelled as some combination of cells, EPS,

and external liquid, with each phase considered to be a fluid [17, 25, 39–41]. Applying conservation of mass and momentum for each fluid phase then enables the mechanics of each fluid, and interactions between phases, to be taken into account. Similar multi-phase models have been used in other biological contexts, for example the crawling of individual cells [42], tissue engineering [43–45], and tumour growth [46]. Of particular interest to the problem of a spreading biofilm is the model of Ward and King [47], who treat a bacterial biofilm as a multi-phase mixture of cells and water. They then apply appropriate thin-film limits to derive a model for the early-time spread of a bacterial colony immersed in a nutrient-rich liquid culture medium. A recent paper by Srinivasan, Kaplan, and Mahadevan [48] adopts a similar approach. In their work, the substratum supplies nutrients to the biofilm, and they assume that expansion is driven by osmotic swelling and nutrient availability. They then compare mathematical model predictions with experiments.

Although Srinivasan, Kaplan, and Mahadevan [48] consider the effect of ECM mechanics and nutrient-limitation, their model assumes strong adhesion between the biofilm and substratum. As a result, flow is driven by osmotic stress and a large pressure that must be balanced with a comparatively large surface tension. In contrast, the sliding motility mechanism hypothesised for *S. cerevisiae* involves increased cell surface hydrophobicity, and hence weak adhesion between the biofilm and agar. The extensional flow approach of Ward and King [47] has closer relevance to sliding motility, but in their model the biofilm is immersed in a nutrient-rich liquid culture medium. This is unlike *S. cerevisiae* mats, which receive nutrients from the agar substratum; their ability to spread therefore depends on the supply of a depleting nutrient, which is also relevant to biofilm growth in nature or in a human host [49]. Ward and King [47] also only consider early biofilm development, and thus neglect the production of ECM, which becomes important on the time scale of our experiments. Furthermore, multi-phase fluid models have also only previously been applied to bacterial biofilms, rather than the fungal biofilms considered here. Based on these considerations, in this work, we aim to extend the multi-phase fluid model of Ward and King [47], to model *S. cerevisiae* mat formation experiments.

2 Mathematical model

We consider growth of a yeast biofilm in cylindrical co-ordinates (r, θ, z), and assume radial symmetry from the outset. The biofilm occupies the region $0 < r < S(t)$ and $0 < z < h(r, t)$, where the leading edge of the biofilm $S(t)$ is termed the contact line, and $h(r, t)$ represents the free upper surface of the biofilm. We define H_b and R_b to be the characteristic height and radius of biofilm growth respectively. The biofilm grows on a substratum, which has depth H_s and is assumed rigid. A sketch of the problem domain,

which closely resembles that of Ward and King [47], is shown in Figure 2.1.

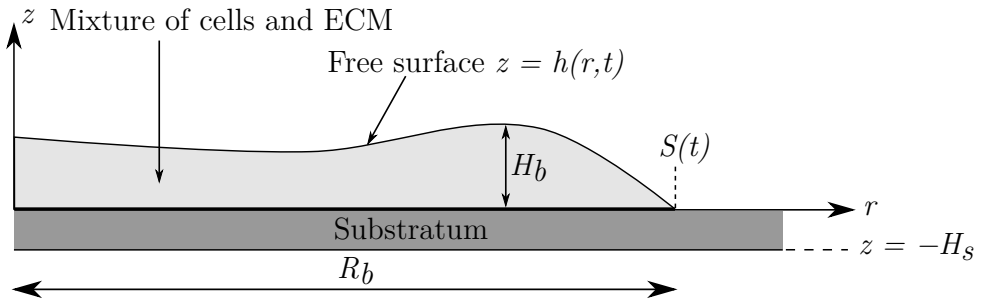

Figure 2.1: A vertical slice through the centre of the biofilm and substratum.

We adopt a macroscopic continuum model, and treat the biofilm as a mixture of two viscous fluid phases. These comprise a living cell phase denoted with the subscript n, and an ECM phase denoted with the subscript m. We define the volume fractions of living cells and ECM to be $\phi_n(r,z,t)$ and $\phi_m(r,z,t)$ respectively, and assume that the mixture contains no voids, that is

$$\phi_n + \phi_m = 1. \tag{2.1}$$

In defining these volume fractions, we note that it is not possible for both species to occupy the same space simultaneously. Throughout this work, we implicitly assume that an appropriate averaging process has taken place, and do not discuss the details here. We direct the reader to the paper by Drew [50] for further information.

A novelty of our approach is that unlike many previous models, we incorporate the effect of nutrient limitation in addition to biofilm mechanics. To enable this, we define $g_s(r,z,t)$ defined for $-H_s < z < 0$, to be the nutrient concentration in the substratum, and $g_b(r,z,t)$ defined for $0 < z < h(r,t)$ and $0 < r < S(t)$, to be the nutrient concentration in the biofilm. After deriving the governing equations, we impose the initial and boundary conditions required to close the model in §2.2. Nutrients can enter the biofilm across the biofilm–substratum interface, at which point they become available for consumption by the cells. This, combined with boundary conditions for the fluid flow, completes our description of sliding motility in biofilms.

2.1 Governing equations

We derive the governing equations of our general model using conservation of mass and momentum. For the mass balances, we assume that the density of each fluid phase is constant, and that the mass flux of each phase is entirely advective. The mass balance equations then read

$$\frac{\partial \phi_\alpha}{\partial t} + \frac{1}{r}\frac{\partial}{\partial r}\left(r u_{r\alpha}\phi_\alpha\right) + \frac{\partial}{\partial z}\left(u_{z\alpha}\phi_\alpha\right) = J_\alpha, \tag{2.2}$$

where $\boldsymbol{u}_\alpha = (u_{r\alpha}, u_{z\alpha})$ for $\alpha = n, m$, are the fluid velocities. The J_α terms represent the net volumetric source of phase α. For these terms, we adapt the bilinear forms used in Tam et al. [5] to include cell death. Assuming that dead cells immediately become part of the ECM, we write

$$J_n = \psi_n \phi_n g_b - \psi_d \phi_n, \quad J_m = \psi_m \phi_n g_b + \psi_d \phi_n, \tag{2.3}$$

where ψ_n is the cell production rate, ψ_m is the ECM production rate, and ψ_d is the cell death rate, all of which are constant. In (2.3), cell death is proportional to cell density only, while production of both living cells and ECM increases with local cell density and nutrient concentration. This is consistent with experimental observations, which show that cellular components and ECM are both formed by catabolism of cellular synthesised glucose [51]. Despite not being considered here, our model also retains the possibility of incorporating more complicated mechanisms, for example ECM production regulated by quorum sensing [40].

We assume that nutrients disperse by diffusion in the substratum, and by both diffusion and advection with extracellular fluid inside the biofilm. As in Tam et al. [5], we assume that the rate at which nutrients are consumed is proportional to the local density of cells and nutrients. The mass balance equations for the nutrients in the substratum and biofilm respectively then read

$$\frac{\partial g_s}{\partial t} = D_s \left[\frac{1}{r} \frac{\partial}{\partial r} \left(r \frac{\partial g_s}{\partial r} \right) + \frac{\partial^2 g_s}{\partial z^2} \right], \tag{2.4}$$

$$\frac{\partial g_b}{\partial t} + \frac{1}{r} \frac{\partial}{\partial r} \left[r u_{rm} (1 - \phi_n) g_b \right] + \frac{\partial}{\partial z} \left[u_{zm} (1 - \phi_n) g_b \right] = D_b \left[\frac{1}{r} \frac{\partial}{\partial r} \left(r \frac{\partial g_b}{\partial r} \right) + \frac{\partial^2 g_b}{\partial z^2} \right] - \eta \phi_n g_b, \tag{2.5}$$

where D_s and D_b are the nutrient diffusivities in the substratum and biofilm respectively, and η is the maximum nutrient consumption rate.

Since the biofilm spreads as a unit in sliding motility, we follow O'Dea, Waters, and Byrne [43] and assume strong interphase drag between the cells and the ECM, so that both phases move with the same velocity $\boldsymbol{u}_n = \boldsymbol{u}_m = \boldsymbol{u}$. Then, for simplicity, we assume that the cells and ECM have the same dynamic viscosity μ, so effectively the mixture can be treated as a single viscous fluid. We denote the stress tensor for the mixture by $\boldsymbol{\sigma}$, and since inertial effects are negligible ($\mathrm{Re} \ll 1$) on the time and length scales of biofilm growth, it satisfies the momentum balance equation

$$\nabla \cdot \boldsymbol{\sigma} = \mathbf{o}. \tag{2.6}$$

Owing to cell proliferation and death, and ECM production, the stress components for

the mixture will include terms involving $\nabla \cdot \boldsymbol{u}$, which commonly vanish. In cylindrical geometry, the relevant components of the stress tensor are

$$\begin{aligned} \sigma_{rr} &= -p - \frac{2\mu}{3}\nabla\cdot\boldsymbol{u} + 2\mu\frac{\partial u_r}{\partial r}, \quad \sigma_{rz} = \sigma_{zr} = \mu\left(\frac{\partial u_r}{\partial z} + \frac{\partial u_z}{\partial r}\right), \\ \sigma_{\theta\theta} &= -p - \frac{2\mu}{3}\nabla\cdot\boldsymbol{u} + \frac{2\mu}{r}u_r, \quad \sigma_{zz} = -p - \frac{2\mu}{3}\nabla\cdot\boldsymbol{u} + 2\frac{\partial u_z}{\partial z}. \end{aligned} \tag{2.7}$$

where p is the pressure [52]. Note that we have invoked Stokes' hypothesis, giving the standard coefficient $-2\mu/3$ for the divergence terms in (2.7) [47, 53, 54]. Substituting (2.7) into (2.6), we find the momentum balances in the r and z directions respectively are

$$-\frac{\partial p}{\partial r} + \frac{2\mu}{r}\frac{\partial}{\partial r}\left(r\frac{\partial u_r}{\partial r}\right) - \frac{2\mu}{3}\frac{\partial}{\partial r}\left[\frac{1}{r}\frac{\partial}{\partial r}(ru_r) + \frac{\partial u_z}{\partial z}\right] + \mu\frac{\partial}{\partial z}\left(\frac{\partial u_z}{\partial r} + \frac{\partial u_r}{\partial z}\right) - \frac{2\mu}{r^2}u_r = 0, \tag{2.8a}$$

$$-\frac{\partial p}{\partial z} + 2\mu\frac{\partial^2 u_z}{\partial z^2} - \frac{2\mu}{3}\frac{\partial}{\partial z}\left[\frac{1}{r}\frac{\partial}{\partial r}(ru_r) + \frac{\partial u_z}{\partial z}\right] + \frac{\mu}{r}\frac{\partial}{\partial r}\left[r\left(\frac{\partial u_r}{\partial z} + \frac{\partial u_z}{\partial r}\right)\right] = 0. \tag{2.8b}$$

Given appropriate initial and boundary conditions, these momentum balance equations (2.8), together with the mass balance equations (2.2), (2.4) and (2.5), define a closed system of governing equations for the fluid pressure, fluid velocity, and nutrient concentrations.

2.2 Initial and boundary conditions

To close the system of governing equations, we require initial and boundary conditions for all of the physical variables. When constructing the general model, we will leave the initial conditions arbitrary. We obtain the first boundary condition by noting that nutrient cannot pass through the base of the substratum. Assuming that the substratum is rigid, the no-flux condition is

$$\frac{\partial g_s}{\partial z} = 0, \quad \text{on} \quad z = -H_s. \tag{2.9}$$

On the biofilm–substratum interface, we assume that the nutrient flux is proportional to the local concentration difference, and impose that fluid cannot pass through the interface. We then have

$$D_s\frac{\partial g_s}{\partial z} = -Q\left(g_s - g_b\right), \quad D_b\frac{\partial g_b}{\partial z} = -Q\left(g_s - g_b\right), \quad u_z = 0 \quad \text{on} \quad z = 0. \tag{2.10}$$

In equations (2.10), the constant Q is the nutrient mass transfer coefficient, which indicates the permeability of the biofilm. To obtain a condition for the fluid velocity on the biofilm–substratum interface, we use the hypothesis that sliding motility increases surface hydrophobicity, causing weak adhesion between the biofilm and substratum [6]. To model this, we impose zero tangential stress on the biofilm–substratum interface instead of the

more common no-slip condition. The boundary condition reads

$$\hat{\boldsymbol{t}} \cdot (\phi_\alpha \boldsymbol{\sigma} \cdot \hat{\boldsymbol{n}}) = \frac{\partial u_r}{\partial z} + \frac{\partial u_z}{\partial r} = 0 \quad \text{on} \quad z = 0, \tag{2.11}$$

where $\hat{\boldsymbol{t}}$ is any unit tangent vector, and $\hat{\boldsymbol{n}}$ is the unit outward normal vector.

For the boundary conditions on the free surface, we first observe that nutrient cannot pass through the biofilm–air interface. This yields the no-flux condition

$$(g_b \phi_m \boldsymbol{u}_m - D_b \nabla g_b) \cdot \hat{\boldsymbol{n}} = 0 \quad \text{on} \quad z = h. \tag{2.12}$$

On each fluid phase we also impose the kinematic condition

$$\frac{\partial h}{\partial t} + u_r \frac{\partial h}{\partial r} = u_z \quad \text{on} \quad z = h, \tag{2.13}$$

which states that fluid particles on the free surface must remain there. Finally, we obtain stress boundary conditions by noting that a free surface is subject to zero tangential stress, and normal stress that is proportional to its local curvature. In general, these conditions read

$$\hat{\boldsymbol{t}} \cdot (\phi_\alpha \boldsymbol{\sigma} \cdot \hat{\boldsymbol{n}}) = 0, \quad \hat{\boldsymbol{n}} \cdot (\phi_\alpha \boldsymbol{\sigma} \cdot \hat{\boldsymbol{n}}) = -\gamma\kappa \quad \text{on} \quad z = h, \tag{2.14}$$

where γ is the surface tension coefficient, and $\kappa = \nabla \cdot \hat{\boldsymbol{n}}$, for the free surface normal vector $\hat{\boldsymbol{n}} = (-h_r, 1) / (1 + h_r^2)^{-1/2}$ (where subscripts here denote partial differentiation), is the mean free surface curvature. This completes the boundary conditions associated with the model.

3 Extensional flow thin-film approximation

In this section, we use a thin-film approximation to obtain a simplified approximation to the model derived in §2. A key observation is that the radius of a biofilm significantly exceeds both its height and the depth of the substratum. This allows us to assume that the aspect ratio $H_s/R_b = \varepsilon \ll 1$, as well as $H_b/R_b = \mathcal{O}(\varepsilon)$. In §3.1, we nondimensionalise the governing equations with this in mind. The choice of scaling regime depends on the physics most relevant to the problem. For sliding motility in which surface tension is reduced [6], it is appropriate to model the biofilm as an extensional flow, which was considered by Ward and King [47]. In §3.2 and §3.3 we adopt this approach, and use a thin-film approximation to simplify the governing equations and boundary conditions considerably. We then propose parameter values and source terms in §3.4, yielding a one-dimensional axisymmetric model that we can compare with experimental results.

3.1 Scaling and nondimensionalisation

To nondimensionalise the equations, we use the initial biofilm radius, R_b, as the length scale, and scale time by the cell production rate, ψ_n, and initial nutrient concentration, G. The scaled variables are (where hats denote dimensionless quantities)

$$\begin{aligned}(r,z) = (R_b\hat{r}, \varepsilon R_b\hat{z}), \quad (u_r,u_z) = (\psi_n G R_b \hat{u_r}, \varepsilon\psi_n G R_b \hat{u_z}),\\ t = \frac{\hat{t}}{\psi_n G}, \quad g_s = G\hat{g}_s, \quad g_b = G\hat{g}_b, \quad p = \psi_n G\mu\hat{p}.\end{aligned} \tag{3.1}$$

Under this scaling, the governing equations (2.2), (2.4), (2.5) and (2.8) become, after dropping hats and eliminating ϕ_m by summing (2.2) over both phases and applying (2.1),

$$\frac{1}{r}\frac{\partial}{\partial r}\left(ru_r\right) + \frac{\partial u_z}{\partial z} = \left(1+\Psi_m\right)\phi_n g_b, \tag{3.2a}$$

$$\frac{\partial \phi_n}{\partial t} + \frac{1}{r}\frac{\partial}{\partial r}\left(ru_r\phi_n\right) + \frac{\partial}{\partial z}\left(u_z\phi_n\right) = \phi_n g_b - \Psi_d\phi_n, \tag{3.2b}$$

$$\frac{\partial g_s}{\partial t} = D\left[\frac{1}{r}\frac{\partial}{\partial r}\left(r\frac{\partial g_s}{\partial r}\right) + \frac{1}{\varepsilon^2}\frac{\partial^2 g_s}{\partial z^2}\right], \tag{3.2c}$$

$$\mathrm{Pe}\left\{\frac{\partial g_b}{\partial t} + \frac{1}{r}\frac{\partial}{\partial r}\left[ru_r\left(1-\phi_n\right)g_b\right] + \frac{\partial}{\partial z}\left[u_z\left(1-\phi_n\right)g_b\right]\right\} = \frac{1}{r}\frac{\partial}{\partial r}\left(r\frac{\partial g_b}{\partial r}\right) + \frac{1}{\varepsilon^2}\frac{\partial^2 g_b}{\partial z^2} - \Upsilon\phi_n g_b, \tag{3.2d}$$

$$-\frac{\partial p}{\partial r} + \frac{2}{r}\frac{\partial}{\partial r}\left(r\frac{\partial u_r}{\partial r}\right) - \frac{2}{3}\frac{\partial}{\partial r}\left[\frac{1}{r}\frac{\partial}{\partial r}\left(ru_r\right) + \frac{\partial u_z}{\partial z}\right] + \frac{\partial}{\partial z}\left(\frac{\partial u_z}{\partial r} + \frac{1}{\varepsilon^2}\frac{\partial u_r}{\partial z}\right) - \frac{2u_r}{r^2} = 0, \tag{3.2e}$$

$$-\frac{\partial p}{\partial z} + 2\frac{\partial^2 u_z}{\partial z^2} - \frac{2}{3}\frac{\partial}{\partial z}\left[\frac{1}{r}\frac{\partial}{\partial r}\left(ru_r\right) + \frac{\partial u_z}{\partial z}\right] + \frac{1}{r}\frac{\partial}{\partial r}\left[r\left(\frac{\partial u_r}{\partial z} + \varepsilon^2\frac{\partial u_z}{\partial r}\right)\right] = 0, \tag{3.2f}$$

where we have introduced the dimensionless constants

$$\Psi_m = \frac{\psi_m}{\psi_n}, \quad \Psi_d = \frac{\psi_d G}{\psi_n}, \quad D = \frac{D_s}{\psi_n G R_b^2}, \quad \mathrm{Pe} = \frac{\psi_n G R_b^2}{D_b}, \quad \text{and} \quad \Upsilon = \frac{\eta R_b^2}{D_b}. \tag{3.3}$$

In (3.3), Ψ_m and Ψ_d are the dimensionless ECM production and cell death rates respectively. The parameter D is the coefficient of diffusion for nutrients in the substratum, scaled by the cell production rate and biofilm radius. The Péclet number, Pe, is the ratio of the rates of advective transport to diffusive transport within the biofilm. The parameter Υ is the dimensionless nutrient consumption rate. We scale Υ differently to the corresponding term in Ward and King [47]. In their model, the biofilm was immersed in a nutrient-rich liquid culture medium, and hence they balanced nutrient consumption with diffusion in the z-direction. In contrast, *S. cerevisiae* mats grow on a nutrient-limited thin substratum, making it appropriate to balance nutrient consumption with the temporal derivative and

in-plane advection and diffusion.

Applying the same scaling (3.1), the dimensionless boundary conditions are

$$\frac{\partial g_s}{\partial z} = 0, \quad \text{on} \quad z = -1, \tag{3.4a}$$

$$\frac{\partial g_s}{\partial z} = -\varepsilon^2 Q_s \left(g_s - g_b\right), \quad \frac{\partial g_b}{\partial z} = -\varepsilon^2 Q_b \left(g_s - g_b\right) \quad \text{on} \quad z = 0, \tag{3.4b}$$

$$\frac{\partial u_r}{\partial z} + \varepsilon^2 \frac{\partial u_z}{\partial r} = 0, \quad \text{on} \quad z = 0, \tag{3.4c}$$

$$u_z = 0 \quad \text{on} \quad z = 0, \quad u_z = \frac{\partial h}{\partial t} + u_r \frac{\partial h}{\partial r} \quad \text{on} \quad z = h, \tag{3.4d}$$

$$\mathrm{Pe}\left[g_b \left(1 - \phi_n\right)\left(u_r \frac{\partial h}{\partial r} - u_z\right)\right] = \frac{\partial g_b}{\partial r}\frac{\partial h}{\partial r} - \frac{1}{\varepsilon^2}\frac{\partial g_b}{\partial z} \quad \text{on} \quad z = h, \tag{3.4e}$$

$$-2\frac{\partial h}{\partial r}\left(\frac{\partial u_r}{\partial r} - \frac{\partial u_z}{\partial z}\right) + \frac{1}{\varepsilon^2}\frac{\partial u_r}{\partial z} + \frac{\partial u_z}{\partial r} - \left(\frac{\partial h}{\partial r}\right)^2 \left(\varepsilon^2 \frac{\partial u_z}{\partial r} + \frac{\partial u_r}{\partial z}\right) = 0 \quad \text{on} \quad z = h, \tag{3.4f}$$

$$\begin{aligned} -p + 2\left[\varepsilon^2 \left(\frac{\partial h}{\partial r}\right)^2 + 1\right]^{-1} \left[\varepsilon^2 \left(\frac{\partial h}{\partial r}\right)^2 \frac{\partial u_r}{\partial r} - \frac{\partial h}{\partial r}\left(\frac{\partial u_r}{\partial z} + \varepsilon^2 \frac{\partial u_z}{\partial r}\right) + \frac{\partial u_z}{\partial z}\right] \\ - \frac{2}{3}\left[\frac{1}{r}\frac{\partial}{\partial r}\left(r u_r\right) + \frac{\partial u_z}{\partial z}\right] = -\gamma^* \kappa^* \quad \text{on} \quad z = h, \end{aligned} \tag{3.4g}$$

where κ^* is the dimensionless mean free surface curvature. The dimensionless parameters,

$$Q_s = \frac{Q R_b}{\varepsilon D_s}, \quad Q_b = \frac{Q R_b}{\varepsilon D_b}, \quad \text{and} \quad \gamma^* = \frac{\varepsilon \gamma}{\psi_n G R_b \mu}, \tag{3.5}$$

are all assumed to be $\mathcal{O}(1)$. The mass transfer parameters Q_s and Q_b are the nutrient depletion rate (from the substratum), and nutrient uptake rate (by the biofilm) respectively. The dimensionless surface tension coefficient (or inverse capillary number), γ^*, is the ratio of surface tension forces to viscous forces. Equations (3.2), and the boundary conditions (3.4), then complete the dimensionless extensional flow model, on which we apply the thin-film reduction.

3.2 Thin-film equations

We now use a thin-film approximation to simplify the dimensionless extensional flow model derived in §3.1. This involves expanding the dependent variables in powers of ε^2,

$$h(r,t) \sim h_0(r,t) + \varepsilon^2 h_1(r,t) + \mathcal{O}\left(\varepsilon^4\right), \tag{3.6a}$$

$$\phi_n(r,z,t) \sim \phi_{n0}(r,z,t) + \varepsilon^2 \phi_{n1}(r,z,t) + \mathcal{O}\left(\varepsilon^4\right), \tag{3.6b}$$

and so on, where series for p, u_r, u_z, g_s, and g_b take the same form as (3.6b). Substituting (3.6) into the dimensionless governing equations (3.2), at leading order we obtain

$$\frac{1}{r}\frac{\partial}{\partial r}\left(ru_{r0}\right)+\frac{\partial u_{z0}}{\partial z}=\left(1+\Psi_m\right)\phi_{n0}g_{b0}, \tag{3.7a}$$

$$\frac{\partial \phi_{n0}}{\partial t}+\frac{1}{r}\frac{\partial}{\partial r}\left(r\phi_{n0}u_{r0}\right)+\frac{\partial}{\partial z}\left(\phi_{n0}u_{z0}\right)=\phi_{n0}g_{b0}-\Psi_d\phi_{n0}, \tag{3.7b}$$

$$\frac{\partial^2 g_{s0}}{\partial z^2}=\frac{\partial^2 g_{b0}}{\partial z^2}=0, \tag{3.7c}$$

$$\frac{\partial^2 u_{r0}}{\partial z^2}=0, \tag{3.7d}$$

$$-\frac{\partial p_0}{\partial z}+\frac{1}{3}\frac{\partial}{\partial z}\left[\frac{1}{r}\frac{\partial}{\partial r}\left(ru_{r0}\right)+\frac{\partial u_{z0}}{\partial z}\right]+\frac{\partial^2 u_{z0}}{\partial z^2}=0. \tag{3.7e}$$

These are subject to the leading order boundary conditions

$$\frac{\partial g_{s0}}{\partial z}=0 \quad \text{on} \quad z=-1,0, \quad \text{and} \quad \frac{\partial g_{b0}}{\partial z}=0 \quad \text{on} \quad z=0,h_0, \tag{3.8a}$$

$$\frac{\partial u_{r0}}{\partial z}=0 \quad \text{on} \quad z=0,h_0, \quad \text{and} \quad u_{z0}=0 \quad \text{on} \quad z=0, \tag{3.8b}$$

$$\frac{\partial h_0}{\partial t}+u_{r0}\frac{\partial h_0}{\partial r}=u_{z0} \quad \text{on} \quad z=h_0, \tag{3.8c}$$

$$-p_0-\frac{2}{3r}\frac{\partial}{\partial r}\left(ru_{r0}\right)+\frac{4}{3}\frac{\partial u_{z0}}{\partial z}=\frac{\gamma^*}{r}\frac{\partial}{\partial r}\left(r\frac{\partial h_0}{\partial r}\right) \quad \text{on} \quad z=h_0, \tag{3.8d}$$

where the rightmost term in (3.8d) incorporates $\kappa^*=\nabla^2 h_0$, which is the leading order local free surface curvature.

Equations (3.7c) and (3.7d) and the associated boundary conditions (3.8a) and (3.8b) demonstrate that g_{s0}, g_{b0}, and u_{r0} are independent of z, as is characteristic of extensional flows. In a similar way to, for example King and Oliver [55], we exploit this by integrating the governing equations with respect to z across the biofilm depth to derive a one-dimensional closed system of equations for the leading order variables. First, we introduce the depth-averaged cell volume fraction

$$\bar{\phi}_{n0}=\frac{1}{h_0}\int_0^{h_0}\phi_{n0}\,\mathrm{d}z. \tag{3.9}$$

Integration of (3.7a) and (3.7b) with respect to z then yields, after application of Leibniz's

integral rule in (3.7b),

$$\frac{\partial h_0}{\partial t} + \frac{1}{r}\frac{\partial}{\partial r}\left(r u_{r0} h_0\right) = \left(1 + \Psi_m\right)\bar{\phi}_{n0} g_{b0} h_0, \tag{3.10a}$$

$$\frac{\partial}{\partial t}\left(\bar{\phi}_{n0} h_0\right) + \frac{1}{r}\frac{\partial}{\partial r}\left(r u_{r0}\bar{\phi}_{n0} h_0\right) = \left(\bar{\phi}_{n0} g_{b0} - \Psi_d \bar{\phi}_{n0}\right) h_0, \tag{3.10b}$$

where subtracting (3.10a) from (3.10b) gives

$$\frac{\partial \bar{\phi}_{n0}}{\partial t} + u_{r0}\frac{\partial \bar{\phi}_{n0}}{\partial r} = \bar{\phi}_{n0}\left[g_{b0} - \Psi_d - \left(1 + \Psi_m\right)\bar{\phi}_{n0} g_{b0}\right]. \tag{3.11}$$

To obtain equations for the leading order nutrient concentrations, we need to consider the higher order correction terms to the governing equations (3.2c) and (3.2d). Upon substituting the expansions (3.6), the $\mathcal{O}(1)$ balances are

$$\frac{\partial^2 g_{s1}}{\partial z^2} = \frac{1}{D}\frac{\partial g_{s0}}{\partial t} - \frac{1}{r}\frac{\partial}{\partial r}\left(r\frac{\partial g_{s0}}{\partial r}\right), \tag{3.12a}$$

$$\begin{aligned}\frac{\partial^2 g_{b1}}{\partial z^2} = \mathrm{Pe}\left\{\frac{\partial g_{b0}}{\partial t} + \frac{1}{r}\frac{\partial}{\partial r}\left[r u_{r0}(1-\phi_{n0}) g_{b0}\right] + \frac{\partial}{\partial z}\left[u_{z0}(1-\phi_{n0}) g_{b0}\right]\right\} \\ - \frac{1}{r}\frac{\partial}{\partial r}\left(r\frac{\partial g_{b0}}{\partial r}\right) + \Upsilon \phi_{n0} g_{b0}.\end{aligned} \tag{3.12b}$$

Using (3.4a), (3.4b) and (3.4e), we can also obtain higher order corrections to the boundary conditions, giving

$$\frac{\partial g_{s1}}{\partial z} = 0 \quad \text{on} \quad z = -1, \tag{3.13a}$$

$$\frac{\partial g_{s1}}{\partial z} = -Q_s\left(g_{s0} - g_{b0}\right), \quad \frac{\partial g_{b1}}{\partial z} = -Q_b\left(g_{s0} - g_{b0}\right) \quad \text{on} \quad z = 0, \tag{3.13b}$$

$$\frac{\partial g_{b1}}{\partial z} = \frac{\partial g_{b0}}{\partial r}\frac{\partial h_0}{\partial r} - \mathrm{Pe} g_{b0}\left(1 - \phi_{n0}\right)\left(u_{r0}\frac{\partial h_0}{\partial r} - u_{z0}\right) \quad \text{on} \quad z = h_0. \tag{3.13c}$$

Integrating (3.12a) and (3.12b) with respect to z across the substratum and biofilm depth respectively, and applying the boundary conditions (3.13), we obtain

$$\frac{\partial g_{s0}}{\partial t} = D\left[\frac{1}{r}\frac{\partial}{\partial r}\left(r\frac{\partial g_{s0}}{\partial r}\right) - Q_s\left(g_{s0} - g_{b0}\right)\right], \tag{3.14a}$$

$$\mathrm{Pe}\left\{h_0\frac{\partial g_{b0}}{\partial t} + \frac{1}{r}\frac{\partial}{\partial r}\left[r u_{r0}\left(1 - \bar{\phi}_{n0}\right) g_{b0} h_0\right]\right\} = \frac{1}{r}\frac{\partial}{\partial r}\left(r h_0\frac{\partial g_{b0}}{\partial r}\right) + Q_b\left(g_{s0} - g_{b0}\right) - \Upsilon\bar{\phi}_{n0} g_{b0} h_0, \tag{3.14b}$$

for $0 < r < S(t)$. We also need to take into account that the nutrient concentration in the substratum can be non-zero outside of the biofilm domain. Outside of the biofilm, the

nutrient will disperse via diffusion only, and therefore the mass balance equation outside of the biofilm is

$$\frac{\partial g_{s0}}{\partial t} = \frac{D}{r}\frac{\partial}{\partial r}\left(r\frac{\partial g_{s0}}{\partial r}\right), \quad \text{on} \quad S(t) < r < R, \tag{3.15}$$

where $R = R_p/R_b$, and R_p is the radius of the Petri dish. We then seek a solution for g_{s0} such that the nutrient concentration and its first spatial derivative are both continuous at the contact line. Equations (3.14) and (3.15) then constitute the leading order nutrient balance equations for our thin-film model.

Finally, we consider the higher order correction term in the radial momentum equation (3.2e) to obtain equations for the leading order radial velocity. Using the conservation of mass equation (3.2a) to simplify, the relevant term is

$$\frac{\partial^2 u_{r1}}{\partial z^2} = \frac{\partial p_0}{\partial r} + \frac{2}{3}\left(1+\Psi_m\right)\frac{\partial}{\partial r}\left(\phi_{n0}g_{b0}\right) - \frac{2}{r}\frac{\partial}{\partial r}\left(r\frac{\partial u_{r0}}{\partial r}\right) - \frac{\partial}{\partial r}\left(\frac{\partial u_{z0}}{\partial z}\right) + \frac{2u_{r0}}{r^2} \tag{3.16}$$

Similarly, the higher order corrections to the boundary conditions (3.4c) and (3.4f) are

$$\frac{\partial u_{r1}}{\partial z} = 0, \quad \text{on} \quad z = 0, \quad \frac{\partial u_{r1}}{\partial z} = 2\frac{\partial h_0}{\partial r}\left(\frac{\partial u_{r0}}{\partial r} - \frac{\partial u_{z0}}{\partial z}\right) - \frac{\partial u_{z0}}{\partial r} \quad \text{on} \quad z = h_0, \tag{3.17}$$

To evaluate (3.16), we need to solve for the pressure p_0. As u_{r0} is independent of z, integration of (3.7e) with respect to z yields, after applying (3.8d) and using (3.7a),

$$p_0 = \frac{4}{3}\left(1+\Psi_m\right)\phi_{n0}g_{b0} - \frac{2}{r}\frac{\partial}{\partial r}\left(ru_{r0}\right) - \frac{\gamma^*}{r}\frac{\partial}{\partial r}\left(r\frac{\partial h_0}{\partial r}\right). \tag{3.18}$$

Now, integrating (3.16) with respect to z across the biofilm depth, and applying the boundary conditions (3.8c) and (3.17), we obtain

$$4\frac{\partial}{\partial r}\left[\frac{h_0}{r}\frac{\partial}{\partial r}\left(ru_{r0}\right)\right] - \frac{2u_{r0}}{r}\frac{\partial h_0}{\partial r} = 2\left(1+\Psi_m\right)\frac{\partial}{\partial r}\left(\bar{\phi}_{n0}g_{b0}h_0\right) - \gamma^* h_0\frac{\partial}{\partial r}\left[\frac{1}{r}\frac{\partial}{\partial r}\left(r\frac{\partial h_0}{\partial r}\right)\right]. \tag{3.19}$$

The equations (3.10a), (3.11), (3.14), (3.15) and (3.19) then form a closed system for the leading order biofilm height, (depth-averaged) cell volume fraction, nutrient concentrations, and radial fluid velocity. These equations form our one-dimensional, thin-film extensional flow model.

3.3 Initial and boundary conditions

We use experimental observations to propose initial and boundary conditions for the one-dimensional axisymmetric model. The experiments and procedure used in this work

are described in Tam et al. [5]. In the experiments, the Petri dish is initially filled uniformly with nutrient, and a small droplet containing cells and fluid is inoculated in the centre of the dish using a pipette. The fluid in the droplet is rapidly absorbed into the agar substratum, leaving a thin layer of cells, which we assume adopts a parabolic profile. Experiments of *C. albicans* show that extracellular material only emerges in mature biofilm [56], hence we assume the biofilm is initially made up of cells only. Appropriate initial conditions are therefore

$$S(0) = 1, \quad h_0(r,0) = H_0\left(1 - r^2\right), \quad \bar{\phi}_{n0}(r,0) = 1, \quad g_{s0}(r,0) = 1, \quad g_{b0}(r,0) = 0, \tag{3.20}$$

where H_0 is the initial biofilm height, which we expect to be $\mathcal{O}(\varepsilon)$. In specifying (3.20), we note that we have chosen the characteristic length scales to be the initial biofilm height and radius, and scale both nutrient concentrations by the initial concentration in the substratum.

For the boundary conditions, we first assume that the biofilm and nutrient concentration are radially symmetric, and that the centre of the biofilm is fixed. This yields the conditions

$$\left.\frac{\partial h_0}{\partial r}\right|_{(0,t)} = 0, \quad \left.\frac{\partial \bar{\phi}_{n0}}{\partial r}\right|_{(0,t)} = 0, \quad \left.\frac{\partial g_{s0}}{\partial r}\right|_{(0,t)} = 0, \quad \left.\frac{\partial g_{b0}}{\partial r}\right|_{(0,t)} = 0, \quad u_{r0}(0,t) = 0. \tag{3.21}$$

In addition, we know that the contact line position $S(t)$ evolves according to the local fluid velocity, that is

$$\frac{\mathrm{d}S}{\mathrm{d}t} = u_{r0}\left(S(t), t\right). \tag{3.22}$$

To close the one-dimensional axisymmetric model, we now require an additional boundary condition for each of the nutrient concentrations, and the fluid velocity. For the nutrient concentration in the substratum, it is natural to impose the no-flux condition

$$\left.\frac{\partial g_{s0}}{\partial r}\right|_{(R,t)} = 0 \tag{3.23}$$

at the boundary of the Petri dish. Regarding the nutrient concentration in the biofilm, we note that the leading edge of the biofilm is rounded by a meniscus, where the height changes over a region in r with $\mathcal{O}(\varepsilon)$ size [57]. This meniscus is not captured under the original thin-film scaling. With this in mind, close to the contact line we consider a re-scaling of the original variables,

$$(r, z) = \left(S(t) + \varepsilon R_b r^{\dagger}, \varepsilon R_b z^{\dagger}\right), \quad (u_{r0}, u_{z0}) = \left(\varepsilon \psi_n G R_b u_{r0}^{\dagger}, \varepsilon \psi_n G R_b u_{z0}^{\dagger}\right). \tag{3.24}$$

With this scaling, the leading order balance for the flux boundary condition (2.12) becomes

(dropping daggers)

$$\frac{\partial g_{b0}}{\partial z} = \frac{\partial g_{b0}}{\partial r}\frac{\partial h_0}{\partial r} \quad \text{on} \quad z = h_0. \tag{3.25}$$

At the contact line, the left-hand side of (3.25) vanishes due to (3.8a), and in general h_0 can depend on r. The boundary condition on the biofilm nutrient concentration is therefore

$$\left.\frac{\partial g_{b0}}{\partial r}\right|_{(S(t),t)} = 0. \tag{3.26}$$

To close the momentum equation (3.19), we impose that the biofilm experiences zero radial stress at the contact line, that is $\sigma_{rr}\left(S(t),t\right) = 0$. Using (3.18) to eliminate the pressure, we find that

$$\sigma_{rr} = 4\frac{\partial u_{r0}}{\partial r} + 2\frac{u_{r0}}{r} - 2\left(1+\Psi_m\right)\phi_{n0}g_{b0} + \frac{\gamma^*}{r}\frac{\partial}{\partial r}\left(r\frac{\partial h_0}{\partial r}\right). \tag{3.27}$$

Integrating (3.27) over the biofilm depth, or noting that $\bar{\phi}_{n0} \to \phi_n$ as $h \to 0$, we then obtain

$$4\frac{\partial u_{r0}}{\partial r} + \frac{2u_{r0}}{r} = 2\left(1+\Psi_m\right)\bar{\phi}_{n0}g_{b0} - \frac{\gamma^*}{r}\frac{\partial}{\partial r}\left(r\frac{\partial h_0}{\partial r}\right), \quad \text{on} \quad (r,t) = \left(S(t),t\right). \tag{3.28}$$

The equations (3.10a), (3.11), (3.14), (3.15) and (3.19), together with the initial conditions (3.20) and boundary conditions (3.21)–(3.23), (3.26) and (3.28), form a closed one-dimensional axisymmetric model for leading order variables. From here onwards, we drop zero subscripts on leading order terms for convenience.

3.4 Parameters

To obtain a set of parameters to use when comparing the model with *S. cerevisiae* mat formation experiments, we require estimates for all dimensional quantities in (3.1), (3.3) and (3.5). To assist with this, we first set $\Psi_m = 1/9$ to ensure that $\phi_n \to 0.9$, as is consistent with experimental observation. For comparison purposes, we also set $\Psi_d = 0$, as cell death rate is difficult to measure, and images from the end of the experiments show that the proportion of dead cells is low. Furthermore, as reduced surface tension is a characteristic of sliding motility [6], we initially consider $\gamma^* = 0$. The experimental design then enables us to estimate all other dimensional parameters, with the exception of ψ_n and η, which we subsequently fit to experimental data. We then obtain the dimensionless parameters listed in Table 3.1. Further details on how each was estimated are available in the electronic supplementary material. The parameter T corresponds to the dimensionless time taken to complete the experiment, and informs the time domain in numerical solutions

Parameter	Value	Source	Parameter	Value	Source
H_0	0.1	Assumption	D	4.34	[58, 59]
Ψ_m	0.111	Observation	Pe	0.953	[60]
Ψ_d	0	Observation	Υ	3.15	Experimental data
R	14.4	Experimental design	Q_b	8.65	[61]
T	15.9	Experimental data	Q_s	2.09	[61]
γ^*	0	Assumption			

Table 3.1: Dimensionless parameters for a yeast (*S. cerevisiae*) biofilm.

to the model. We note that all constants in the right-hand column are $\mathcal{O}(1)$, which justifies the scaling regime employed in the thin-film model.

4 Results and discussion

In this section, we compare the thin-film extensional flow model derived in §3 with experimental data, and then investigate the dependence of the parameters on the speed of biofilm expansion. To achieve this, we undertake the numerical solution of (3.10a), (3.11), (3.14), (3.15) and (3.19) on $r \in [0, R]$, and $t \in [0, T]$, subject to (3.20)–(3.23), (3.26) and (3.28) in §4.1. Doing so with the parameters in Table 3.1 confirms that sliding motility can reproduce experimental results. In §4.2 and 4.3, we then vary the parameters, including cell death rate and surface tension coefficient, to predict the expansion speed and biofilm shape in different conditions.

4.1 Numerical solutions and comparison with experiments

We use a front-fixing method [62] to solve the one-dimensional axisymmetric model. This involves introducing the new variables

$$\xi = \frac{r}{S(t)}, \quad \text{and} \quad \xi_o = \frac{r - S(t)}{R - S(t)}, \tag{4.1}$$

so that the biofilm always inhabits $\xi \in [0, 1]$, and the interval $\xi_o \in [0, 1]$ represents the remainder of the Petri dish not occupied by the biofilm. We then use a Crank–Nicolson scheme to discretise the model. For all nonlinear terms, we linearise using data from the previous time step. At each time step, we solve the governing equations in the same order as they are derived in §3.2. When solving for the nutrient concentration in the substratum, we use data from the previous time step as an initial guess for $g_s(S, t)$ at the current time step. We then solve both (3.14a) and (3.15), and use Newton's method to correct the initial guess, and ensure that the first spatial derivative of g_s is continuous at $r = S(t)$,

which corresponds to $\xi = 1$ and $\xi_o = 0$. We compute solutions using an equispaced grid with $\Delta\xi = \Delta\xi_o = 1.25 \times 10^{-4}$ and $\Delta t \approx 1 \times 10^{-4}$, which ensures adequate convergence with grid spacing and time step size. Further details on the numerical method are provided in the electronic supplementary material.

We compute solutions for the parameters given in Table 3.1 to facilitate comparison with experiments. There is good agreement between the numerical contact line position and the measured radius of the *S. cerevisiae* mats, as shown in Figure 4.1a. Unlike the reaction–diffusion model of Tam et al. [5], Figure 4.1b shows that the extensional flow model produces a non-constant expansion speed. The velocity profile resembles the experimental *B. subtilis* biofilms of Srinivasan, Kaplan, and Mahadevan [48], featuring an initial period of acceleration followed by a deceleration. A likely explanation of the acceleration observed early in biofilm growth is that cells initially proliferate in nutrient-rich conditions. With abundant nutrients, both existing and newly-produced cells are able to proliferate, accelerating expansion. However, as time passes nutrients become depleted in the centre of the colony, as Figures 4.1c and 4.1d show. When this occurs, cell proliferation is mostly confined to the leading edge (see Figure 4.1f), which slows the expansion of the colony. This phenomenon also dictates the shape a biofilm attains as it expands. As Figure 4.1e shows, our model predicts that the biofilm will expand vertically and radially when nutrients are abundant. When nutrients deplete and growth is concentrated near the leading edge, the biofilm stops thickening and can only expand radially. The model even predicts that the height at the centre of the biofilm will begin to decrease slightly, as the advection of mass with the fluid exceeds the net production rate.

4.2 The effect of model parameters on biofilm size

In §4.1, we considered one set of parameters relevant to the *S. cerevisiae* mat formation experiments. However, biofilms can grow in vastly different ways depending on the microbial species and environmental conditions. To predict biofilm growth by sliding motility in a range of experimental conditions, we compute numerical solutions for five days of growth. For each set of solutions, we use the default parameters given in Table 3.1, and vary one parameter at a time over a realistic range. This allows us to isolate the effect of each parameter on biofilm size, and consequently expansion speed. Of the dimensionless parameters, we found that the Petri dish size R and surface tension coefficient γ^* had negligible effect on the biofilm size. Results for other dimensionless parameters and the cell production rate, ψ_n, are shown in Figure 4.2. A vast range of behaviour is possible while keeping dimensionless parameters within one order of unity.

Figures 4.2a and 4.2b describe how fluid production and cell death affect expansion speed. As expected, higher rates of fluid (either living cells or ECM) production result

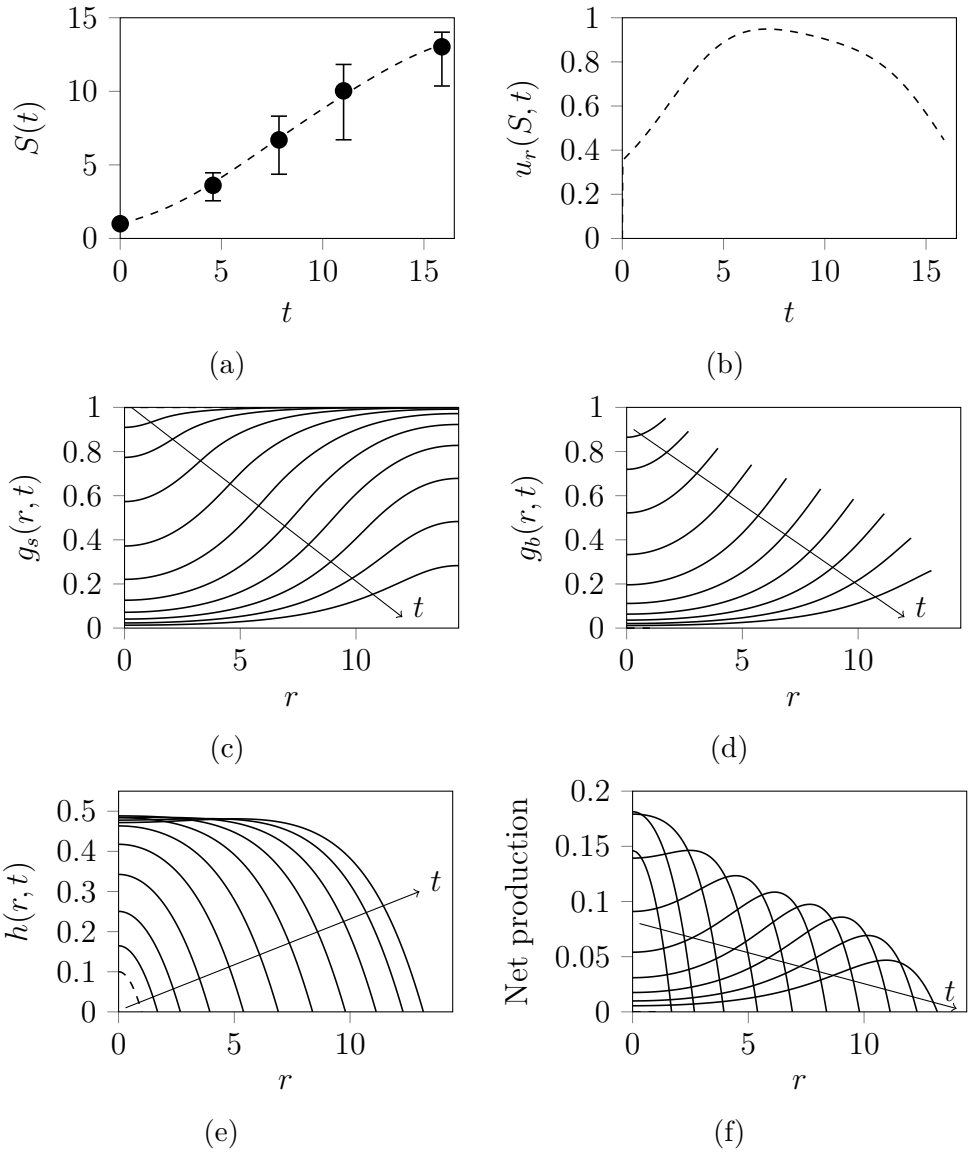

Figure 4.1: Numerical solution and comparison with experimental data. (a) Comparison of numerical contact line position (dashed curve) with experimental data. Dots indicate the mean data, and error bars indicate the experimental range. (b) Instantaneous biofilm expansion speed $u_r(S(t), t)$. (c) Nutrient concentration in the substratum, $g_s(r, t)$. (d) Nutrient concentration in the biofilm $g_b(r, t)$. (e) Biofilm height $h(r, t)$. (f) Net fluid production, $J = (1 + \Psi_m)\,\bar{\phi}_n g_b h$. Figures (c)–(f) are plotted for $t \in [0, 15.9]$, and $r \in [0, 14.4]$, at ten equispaced time intervals. Dashed curves represent initial conditions, and arrows indicate the direction of increasing time.

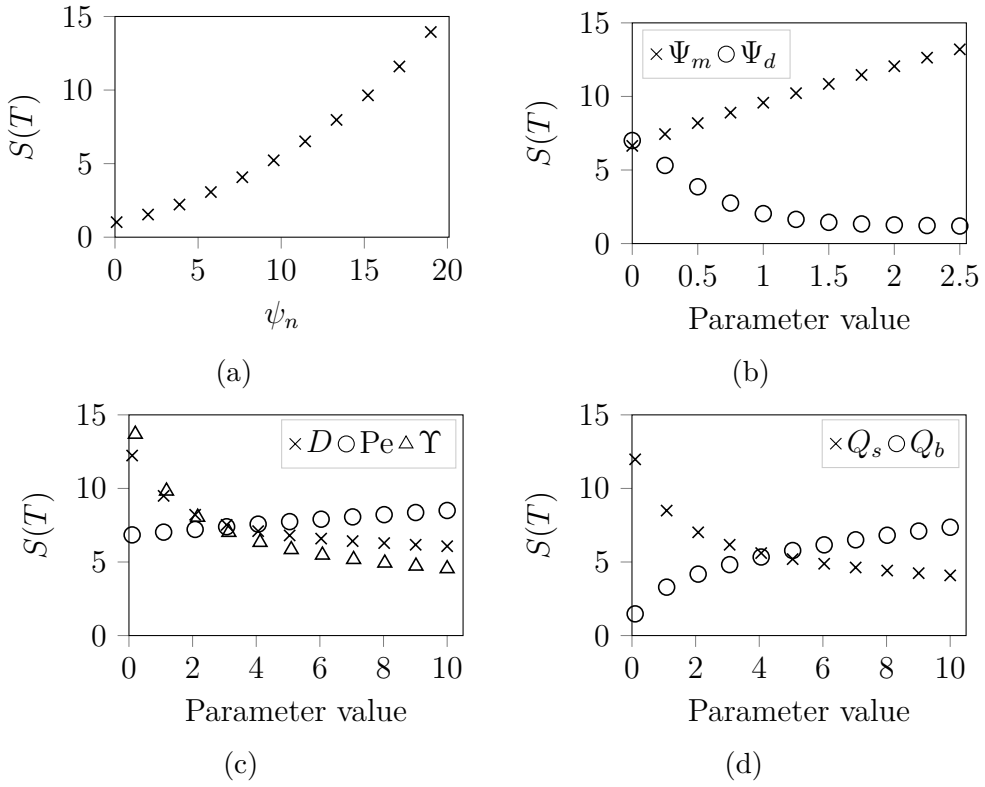

Figure 4.2: The effect of parameters on biofilm radius, $S(T)$, where for each solution T is the dimensionless time corresponding to five days. The initial conditions are (3.20), and parameters (excepting T) where held constant are given in Table 3.1.

in larger biofilms. However, unlike the production of ECM, the production of new cells facilitates increased cell proliferation in the future, and therefore cell production rate is a stronger determinant of size than ECM production rate. This verifies that expansion in sliding motility is mostly driven by cell proliferation. In addition, Figure 4.2b shows that increasing the cell death rate decreases biofilm size, which is expected as fewer living cells are subsequently available to proliferate.

The remaining plots in Figure 4.2 show how the dimensionless parameters affect expansion speed. The effect of nutrient movement and consumption is revealed in Figure 4.2c. Increasing the nutrient diffusion coefficient D will result in more uniform nutrient concentrations across the Petri dish than seen in Figure 4.1c and 4.1d. This promotes thickening of the biofilm as opposed to radial expansion. In addition, increasing the nutrient consumption rate Υ results in larger quantities of nutrient being required to produce a new cell, thereby slowing expansion. Although the Péclet number Pe does not significantly affect expansion speed, larger values imply increased advection of cells and nutrients towards the biofilm edge, which increases expansion speed. Figure 4.2d illustrates the effect of the nutrient depletion and uptake rates. Larger values of nutrient depletion rate Q_s decrease nutrient access to the cells, which slows expansion. Conversely, increasing nutrient uptake rate Q_b aids cell production, as more nutrients become available for consumption. A common theme in all of these results is that expansion speed depends on the ability of cells close to the leading edge to consume nutrient and proliferate. The results presented here are relevant to clinical settings, where expansion speed correlates with the invasiveness of infection. Our model describes environmental conditions that result in decreased expansion speed.

4.3 Predicting biofilm shape: ridge formation and surface tension

In addition to the size, our model also predicts the shape a growing biofilm will attain. Although not observed in *S. cerevisiae* mat formation experiments, some bacterial biofilms [48] and yeast colony biofilms [51] develop a ridge structure close to the leading edge. To observe ridge formation in our model, we compute a numerical solution with the experimental parameters given in Table 3.1, except with $D = 1.5$, $\Upsilon = 10$, and $\mathrm{Pe} = 10$. Compared to the experimental parameters, this combination of decreased nutrient diffusion, and increased nutrient consumption and advection leads to faster nutrient depletion behind the proliferating rim. Cell proliferation then becomes concentrated close to the leading edge, which in conjunction with increased advection of mass outwards from the biofilm centre, creates the noticeable ridge seen in Figure 4.3a. To quantify ridge formation, we compute the normalised ridge height $I_r(t) = (\max h(r,t))/h(0,t)$ in the new numerical solution, and compare with the experimental case. Figure 4.3b shows the normalised ridge

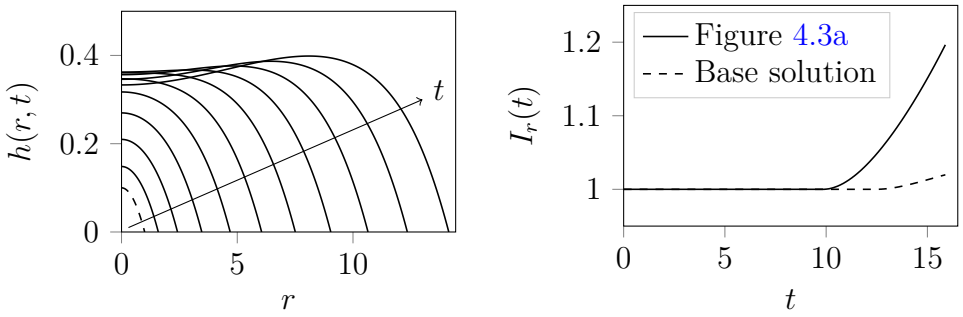

(a) Biofilm height. (b) Normalised ridge height.

Figure 4.3: The solution with $D = 1.5$, $\Upsilon = 10$, and $\mathrm{Pe} = 10$, with other parameters as in Table 3.1.

height increasing faster than the base solution with experimental parameters. Although we do not investigate the mechanisms of ridge formation in detail, our model shows that interplay between sliding motility and nutrient-limited growth can initiate ridge formation. Importantly, this can occur without the need to invoke other mechanisms such as osmotic swelling or mechanical blistering.

Finally, we investigate the effect that non-zero surface tension would have on the biofilm shape. We achieve this by computing numerical solutions with the parameters as in Figure 4.3, while varying the surface tension coefficient over the range $\gamma^* \in [0, 2]$. These results are shown in Figure 4.4. We observe that increasing the surface tension coefficient reduces the extent of the ridge, and that $\gamma^* = 2$ is sufficient to prevent ridge formation. As surface tension appears only in the momentum equation (3.19) and boundary condition (3.28), we expect the fluid velocity profile to explain this behaviour. Figure 4.4c shows that increasing γ^* decreases the radial velocity near the centre of the biofilm. This decreases movement of fluid and nutrients towards the leading edge of the biofilm, thereby inhibiting ridge formation.

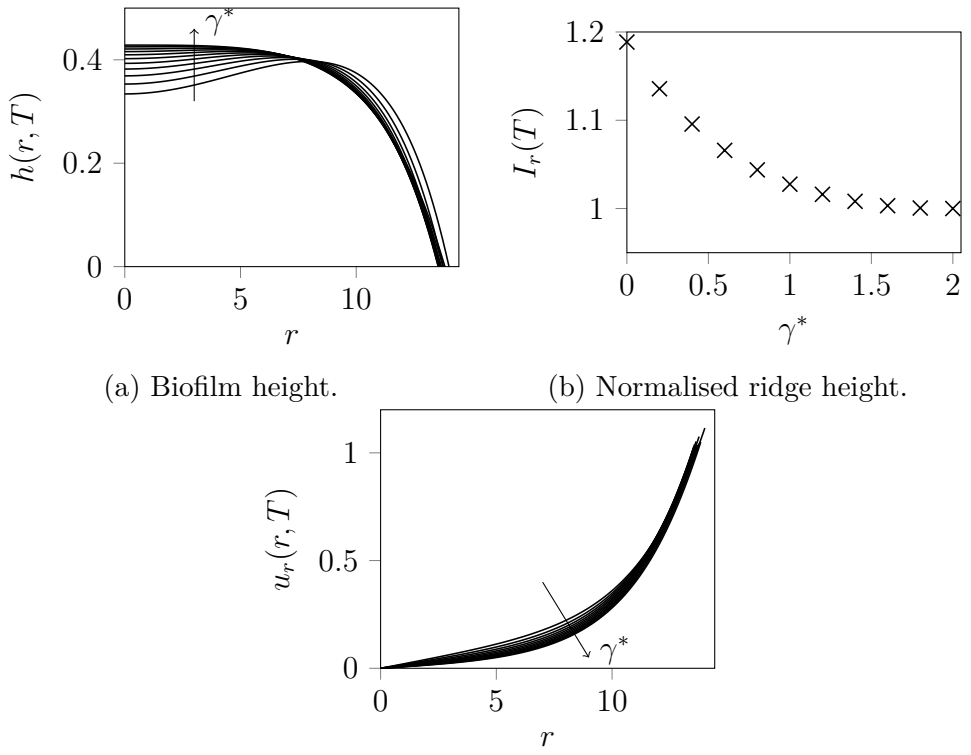

(a) Biofilm height.

(b) Normalised ridge height.

(c) Fluid velocity.

Figure 4.4: Solutions illustrating how surface tension affects ridge formation. The parameters (excepting γ^*) are as in Figure 4.3, and plotted for $\gamma^* \in [0, 2]$, at increments of $\gamma^* = 0.2$.

5 Summary

In this paper, we developed a mathematical model to better understand how mechanics affect yeast biofilm expansion. We were particularly interested in the role of sliding motility and nutrient limitation, features hypothesised to be relevant to mat formation experiments of the budding yeast *S. cerevisiae*. To investigate this, we derived a general multi-phase model for biofilm expansion, treating the biofilm as a mixture of living cells and extracellular fluid. We systematically reduced the model to a one-dimensional axisymmetric form by employing an extensional flow thin-film reduction. By computing numerical solutions, we showed that the thin-film model could reproduce the expansion speed of *S. cerevisiae* mat biofilms. We then confirmed the hypothesis that cell production rate is the strongest determinant of biofilm size in sliding motility. By varying model parameters, we showed that increasing the ability for cells close to the leading edge to consume nutrients and proliferate promotes faster expansion. This can be achieved by decreasing the nutrient diffusion, consumption, and depletion rates, by or increasing nutrient uptake rate. Finally, we showed that sliding motility is a possible explanation for the ridge formation observed in bacterial or yeast colony biofilms. We found that surface tension slows the movement of cells and nutrients towards the biofilm rim, and thus inhibits ridge formation. Our model confirms that sliding motility is a plausible mechanism for yeast biofilm expansion, and offers a way of quantitatively predicting biofilm growth for other microbial species and environmental conditions.

In addition to these results, our model offers an opportunity to study further biological questions. For example, there are potential links between the characteristic floral morphology of *S. cerevisiae* mats and the stability of solutions to azimuthal perturbations. This provides one avenue for further investigation. Depending on the desired application, the general model also retains the possibility of investigating different mechanisms. For example, the model could be re-scaled to investigate expansion driven by strong adhesion and increased surface tension, rather than sliding motility. The model can also incorporate more complicated cell production mechanisms, for example ECM production regulated by quorum sensing. It is also possible to include more complicated mechanical behaviour, for example the viscoelastic rheology of biofilms, the effect of substratum elasticity, or the possibility of expansion by osmotic swelling. We intend to tackle some of these scenarios in future work, to shed further light on the mechanisms governing biofilm expansion.

Acknowledgements

The work used supercomputing resources provided by the Phoenix High Performance Computing service at the University of Adelaide.

Funding

A. T. received funding from the A. F. Pillow Applied Mathematics Trust, and from the Australian Government under the Research Training Program. J. E. F. G., S. B., and B. J. B. acknowledge funding from the Australian Research Council (ARC), under the grants DE130100031, FT130100484, and DP160102644 respectively. E. L. T. was supported by an Adelaide Graduate Research Scholarship and funding from Wine Australia (GWR Ph1305). J. M. G. and J. F. S. were supported by an ARC grant (DP130103547) awarded to V. J.

References

[1] J. D. Murray, *Mathematical Biology II: Spatial Models and Biomedical Applications*, Third, Springer, 2003, DOI: 10.1007/b98869.

[2] A. M. Turing, "The chemical basis of morphogenesis", *Philosophical Transactions of the Royal Society of London* 237 (1952), pp. 37–72, DOI: 10.1098/rstb.1952.0012.

[3] E. F. Keller and L. A. Segel, "Traveling bands of chemotactic bacteria: a theoretical analysis", *Journal of Theoretical Biology* 30 (1971), pp. 235–248, DOI: 10.1016/0022-5193(71)90051-8.

[4] T. B. Reynolds and G. R. Fink, "Bakers' yeast, a model for fungal biofilm formation", *Science* 291 (2001), pp. 878–881, DOI: 10.1126/science.291.5505.878.

[5] A. Tam, J. E. F. Green, S. Balasuriya, E. L. Tek, J. M. Gardner, J. F. Sundstrom, V. Jiranek, and B. J. Binder, "Nutrient-limited growth with non-linear cell diffusion as a mechanism for floral pattern formation in yeast biofilms", *Journal of Theoretical Biology* 448 (2018), pp. 122–141, DOI: 10.1016/j.jtbi.2018.04.004.

[6] R. M. Harshey, "Bacterial motility on a surface: many ways to a common goal", *Annual Review of Microbiology* 57 (2003), pp. 249–273, DOI: 10.1146/annurev.micro.57.030502.091014.

[7] J. Recht, A. Martínez, S. Torello, and R. Kolter, "Genetic analysis of sliding motility in *Mycobacterium smegmatis*", *Journal of Bacteriology* 182 (2000), pp. 4348–4351, DOI: 10.1128/JB.182.15.4348-4351.2000.

[8] L. M. Martinez and B. C. Fries, "Fungal biofilms: relevance in the setting of human disease", *Current Fungal Infection Reports* 4 (2010), pp. 266–275, DOI: 10.1007/s12281-010-0035-5.

[9] H. Flemming and J. Wingender, "The biofilm matrix", *Nature Reviews Microbiology* 8 (2010), pp. 623–633, DOI: 10.1038/nrmicro2415.

[10] G. Ramage, R. Rajendran, L. Sherry, and C. Williams, "Fungal biofilm resistance", *International Journal of Microbiology* (2012), 528521, DOI: 10.1155/2012/528521.

[11] M. S. Lionakis, "New insights into innate immune control of systemic candidiasis", *Medical Mycology* 52 (2014), pp. 555–564, DOI: 10.1093/mmy/myu029.

[12] L. Chen, J. Noorbakhsh, R. M. Adams, J. Samaniego-Evans, G. Agollah, D. Nevozhay, J. Kuzdzal-Fick, P. Mehta, and G. Balázsi, "Two-dimensonality of yeast colony expansion accompanied by pattern formation", *PLOS Computational Biology* 10 (2014), e1003979, DOI: 10.1371/journal.pcbi.1003979.

[13] I. W. Sutherland, "The biofilm matrix — an immobilized but dynamic microbial environment", *Trends in Microbiology* 9 (2001), pp. 222–227, DOI: 10.1016/S0966-842X(01)02012-1.

[14] L. Váchová, V. Štovíček, O. Hlaváček, O. Chernyavskiy, L. Štěpánek, L. Kubínová, and Z. Palková, "Flo11p, drug efflux pumps, and the extracellular matrix cooperate to form biofilm yeast colonies", *Journal of Cell Biology* 194 (2011), pp. 679–687, DOI: 10.1083/jcb.201103129.

[15] A. Beauvais, C. Loussert, M. C. Prevost, K. Verstrepen, and J. P. Latgé, "Characterization of a biofilm-like extracellular matrix in FLO1-expressing *Saccharomyces cerevisiae* cells", *FEMS Yeast Research* 9 (2009), pp. 411–419, DOI: 10.1111/j.1567-1364.2009.00482.x.

[16] T. Shaw, M. Winston, C. J. Rupp, I. Klapper, and P. Stoodley, "Commonality of elastic relaxation times in biofilms", *Physical Review Letters* 93 (2004), 098102, DOI: 10.1103/PhysRevLett.93.098102.

[17] N. G. Cogan and R. D. Guy, "Multiphase flow models of biogels from crawling cells to bacterial biofilms", *Frontiers in Life Sciences* 4 (2010), pp. 11–25, DOI: 10.2976/1.3291142.

[18] A. Goffeau, B. G. Barrell, H. Bussey, R. W. Davis, B. Dujon, H. Feldmann, F. Galibert, J. D. Hoheisel, C. Jacq, M. Johnston, E. J. Louis, H. W. Mewes, Y. Murakami, P. Philippsen, H. Tettelin, and S. G. Oliver, "Life with 6000 Genes", *Science* 274 (1996), pp. 546–567, DOI: 10.1126/science.274.5287.546.

[19] J. R. Blankenship and A. P. Mitchell, "How to build a biofilm: a fungal perspective", *Current Opinion in Microbiology* 9 (2006), pp. 588–594, DOI: 10.1016/j.mib.2006.10.003.

[20] T. R. Hughes, "Yeast and drug discovery", *Functional and Integrative Genomics* 2 (2002), pp. 199–211, DOI: 10.1007/s10142-002-0059-1.

[21] H. Tronnolone, A. Tam, Z. Szenczi, J. E. F. Green, S. Balasuriya, E. L. Tek, J. M. Gardner, J. F. Sundstrom, V. Jiranek, S. G. Oliver, and B. J. Binder, "Diffusion-limited growth of microbial colonies", *Scientific Reports* 8 (2018), pp. 1–11, DOI: 10.1038/s41598-018-23649-z.

[22] A. Seminara, T. E. Angelini, J. N. Wilking, H. Vlamakis, S. Ebrahim, R. Kolter, D. A. Weitz, and M. P. Brenner, "Osmotic spreading of *Bacillus subtilis* biofilms driven by an extracellular matrix", *Proceedings of the National Academy of Sciences of the United States of America* 109 (2012), pp. 1116–1121, DOI: 10.1073/pnas.1109261108.

[23] J. Yan, C. D. Nadell, H. A. Stone, N. S. Wingreen, and B. L. Bassler, "Extracellular-matrix-mediated osmotic pressure drives *Vibrio cholerae* biofilm expansion and cheater exclusion", *Nature Communications* 8 (2017), 327, DOI: 10.1038/s41467-017-00401-1.

[24] M. R. Mattei, L. Frunzo, B. D'Acunto, Y. Pechaud, F. Pirozzi, and G. Esposito, "Continuum and discrete approach in modeling biofilm development and structure: a review", *Journal of Mathematical Biology* 76 (2018), pp. 945–1003, DOI: 10.1007/s00285-017-1165-y.

[25] H. F. Winstanley, M. Chapwanya, M. J. McGuinness, and A. C. Fowler, "A polymer–solvent model of biofilm growth", *Proceedings of the Royal Society of London A* 467 (2010), pp. 1449–1467, DOI: 10.1098/rspa.2010.0327.

[26] C. Picioreanu, M. C. M. van Loosdrecht, and J. J. Heijnen, "Mathematical modeling of biofilm structure with a hybrid differential-discrete cellular automaton approach", *Biotechnology and Bioengineering* 58 (1998), pp. 101–116, DOI: 10.1002/(SICI)1097-0290(19980405)58:1<101::AID-BIT11>3.0.CO;2-M.

[27] S. Matsuura, "Random growth of fungal colony model on diffusive and non-diffusive media", *Forma* 15 (2000), pp. 309–319.

[28] H. Tronnolone, J. M. Gardner, J. F. Sundstrom, V. Jiranek, S. G. Oliver, and B. J. Binder, "Quantifying the dominant growth mechanisms of dimorphic yeast using a lattice-based model", *Journal of the Royal Society Interface* 14 (2017), 20170314, DOI: 10.1098/rsif.2017.0314.

[29] K. Kawasaki, A. Mochizuki, M. Matsushita, T. Umeda, and N. Shigesada, "Modeling spatio-temporal patterns generated by *Bacillus subtilis*", *Journal of Theoretical Biology* 188 (1997), pp. 177–185, DOI: 10.1006/jtbi.1997.0462.

[30] E. Ben-Jacob, I. Cohen, and H. Levine, "Co-operative self organisation in micro-organisms", *Advances in Physics* 49 (2000), pp. 395–554, DOI: 10.1080/000187300405228.

[31] J. Müller and W. van Saarloos, "Morphological instability and dynamics of fronts in bacterial growth models with nonlinear diffusion", *Physical Review E* 65 (2002), 061111, DOI: 10.1103/physreve.65.061111.

[32] A. C. Fowler, T. M. Kyrke-Smith, and H. F. Winstanley, "The development of biofilm architecture", *Proceedings of the Royal Society of London A* 472 (2016), 20150798, DOI: 10.1098/rspa.2015.0798.

[33] O. Wanner and W. Gujer, "A multispecies biofilm model", *Biotechnology and Bioengineering* 28 (1986), pp. 314–328, DOI: 10.1002/bit.260280304.

[34] H. J. Eberl, D. F. Parker, and M. C. M. van Loosdrecht, "A new deterministic spatio-temporal continuum model for biofilm development", *Journal of Theoretical Medicine* 3 (2001), pp. 161–175, DOI: 10.1080/10273660108833072.

[35] I. Klapper and J. Dockery, "Mathematical description of microbial biofilms", *SIAM Review* 52 (2010), pp. 221–265, DOI: 10.1137/080739720.

[36] J. Lega and T. Passot, "Hydrodynamics of bacterial colonies: a model", *Physical Review E* 67 (2003), 031906, DOI: 10.1103/physreve.67.031906.

[37] B. Nguyen, A. Upadhyaya, A. van Oudenaarden, and M. P. Brenner, "Elastic instability in growing yeast colonies", *Biophysical Journal* 86 (2004), pp. 2740–2747, DOI: 10.1016/s0006-3495(04)74327-1.

[38] C. Giverso, M. Verani, and P. Ciarletta, "Branching instability in expanding bacterial colonies", *Journal of the Royal Society Interface* 12 (2015), 20141290, DOI: 10.1098/rsif.2014.1290.

[39] N. G. Cogan and J. P. Keener, "The role of biofilm matrix in structural development", *Mathematical Medicine and Biology* 21 (2004), pp. 147–166, DOI: 10.1093/imammb21.2.147.

[40] K. Anguige, J. R. King, and J. P. Ward, "A multi-phase mathematical model of quorum sensing in a maturing *Pseudomonas aeruginosa* biofilm", *Mathematical Biosciences* 203 (2006), pp. 240–276, DOI: 10.1016/j.mbs.2006.05.009.

[41] F. Clarelli, C. Di Russo, R. Natalini, and M. Ribot, "A fluid dynamics multidimensional model of biofilm growth: stability, influence of environment and sensitivity", *Mathematical Medicine and Biology* (2015), pp. 1–25, DOI: 10.1093/imammb/dqv024.

[42] L. S. Kimpton, J. P. Whiteley, S. L. Waters, and J. M. Oliver, "On a poroviscoelastic model for cell crawling", *Journal of Mathematical Biology* 70 (2015), pp. 133–171, DOI: 10.1007/s00285-014-0755-1.

[43] R. D. O'Dea, S. L. Waters, and H. M. Byrne, "A two-fluid model for tissue growth within a dynamic flow environment", *European Journal of Applied Mathematics* 19 (2008), pp. 607–634, DOI: 10.1017/S0956792508007687.

[44] J. E. F. Green, S. L. Waters, K. M. Shakesheff, and H. M. Byrne, "A mathematical model of liver cell aggregation *In vitro*", *Bulletin of Mathematical Biology* 71 (2009), pp. 906–930, DOI: 10.1007/s11538-008-9387-1.

[45] J. E. F. Green, J. P. Whiteley, J. M. Oliver, H. M. Byrne, and S. L. Waters, "Pattern formation in multiphase models of chemotactic cell aggregation", *Mathematical Medicine and Biology* 35 (2017), pp. 319–346, DOI: 10.1093/imammb/dqx005.

[46] S. R. Lubkin and T. L. Jackson, "Multiphase mechanics of capsule formation in tumors", *Journal of Biomechanical Engineering* 124 (2002), pp. 237–243, DOI: 10.1115/1.1427925.

[47] J. P. Ward and J. R. King, "Thin-film modelling of biofilm growth and quorum sensing", *Journal of Engineering Mathematics* 73 (2012), pp. 71–92, DOI: 10.1007/s10665-011-9490-4.

[48] S. Srinivasan, C. N. Kaplan, and L. Mahadevan, "Dynamics of spreading microbial swarms and films", *BioRxiv* (2018), pre-print, DOI: 10.1101/344267.

[49] Z. Palková and L. Váchová, "Life within a community: benefit to yeast long-term survival", *FEMS Microbiology Reviews* 30 (2006), pp. 806–824, DOI: 10.1111/j.1574-6976.2006.00034.x.

[50] D. A. Drew, "Mathematical modeling of two-phase flow", *Annual Review of Fluid Mechanics* 15 (1983), pp. 261–291, DOI: 10.1146/annurev.fl.15.010183.001401.

[51] J. Maršíková, D. Wilkinson, O. Hlaváček, G. D. Gilfillan, A. Mizeranschi, T. R. Hughes, M. Begany, S. Rešetárová, L. Váchová, and Z. Palková, "Metabolic differentiation of surface and invasive cells of yeast colony biofilms revealed by gene expression profiling", *BMC Genomics* 18 (2017), pp. 1–16, DOI: 10.1186/s12864-017-4214-4.

[52] G. K. Batchelor, *An introduction to fluid dynamics*, Cambridge University Press, 1967.

[53] S. J. Franks, H. M. Byrne, J. R. King, J. C. E. Underwood, and C. E. Lewis, "Modelling the early growth of ductal carcinoma in situ of the breast", *Journal of Mathematical Biology* 47 (2003), pp. 424–452, DOI: 10.1007/s00285-003-0214-x.

[54] R. D. O'Dea, S. L. Waters, and H. M. Byrne, "A multiphase model for tissue construct growth in a perfusion bioreactor", *Mathematical Medicine and Biology* 27 (2010), pp. 95–127, DOI: 10.1093/imammb/dqp003.

[55] J. R. King and J. M. Oliver, "Thin-film modelling of poroviscous free surface flows", *European Journal of Applied Mathematics* 16 (2005), pp. 519–553, DOI: 10.1017/s095679250500584x.

[56] J. Chandra, D. M. Kuhn, P. K. Mukherjee, L. L. Hoyer, T. McCormick, and M. A. Ghannoum, "Biofilm formation by the fungal pathogen *Candida albicans*: development, architecture, and drug resistance", *Journal of Bacteriology* 183 (2001), pp. 5385–5394, DOI: 10.1128/JB.183.18.5385-5394.2001.

[57] P. D. Howell, B. Scheid, and H. A. Stone, "Newtonian pizza: spinning a viscous sheet", *Journal of Fluid Mechanics* 659 (2010), pp. 1–23, DOI: 10.1017/S0022112010001564.

[58] A. L. Slade, A. E. Cremers, and H. C. Thomas, "The obstruction effect in the self-diffusion coefficients of sodium and cesium in agar gels", *Journal of Physical Chemistry* 70 (1966), pp. 2840–2844, DOI: 10.1021/j100881a020.

[59] L. G. Longsworth, "Electrochemistry in biology and medicine", ed. by T. Shedlovsky, John Wiley & Sons, Inc., 1955, chap. 12: Diffusion in liquids and the Stokes–Einstein relation, pp. 225–247, DOI: 10.1016/0002-8703(55)90290-8.

[60] P. S. Stewart, "A review of experimental measurements of effective diffusive permeabilities and effective diffusion coefficients in biofilms", *Biotechnology and Bioengineering* 59 (1998), pp. 261–272, DOI: 10.1002/(SICI)1097-0290(19980805)59:3<261::AID-BIT1>3.0.CO;2-9.

[61] A. A. Vicente, M. Dluhý, E. C. Ferreira, M. Mota, and J. A. Teixeira, "Mass transfer properties of glucose and O_2 in *Saccharomyces cerevisiae* flocs", *Biochemical Engineering Journal* 2 (1998), pp. 35–43, DOI: 10.1016/S1369-703X(98)00015-1.

[62] J. Crank, *Free and moving boundary problems*, Oxford Science Publications, 1984.

A Parameter estimation

To obtain appropriate values for the parameters listed in Table 3.1, we require estimates for all dimensional quantities in (3.1), (3.3) and (3.5). In lieu of an accurate experimental measurement, we will assume that the thin-film parameter $\varepsilon = 0.1$. This is the same value used in the extensional flow model of Ward and King [47], and signifies that the biofilm thickness is an order of magnitude smaller than its radius. Accordingly, we also assume the initial biofilm height is $H_0 = 0.1$.

The experimental design also enables us to estimate several parameters. For example, the mean initial biofilm radius across the thirteen experiments in Tam et al. [5] was $R_b = 2.875\,\text{mm}$. The radius of the medium on which the biofilms were grown was 41.5 mm

[21], giving $R = 14.4$. We use the physical properties of glucose to estimate parameters related to the nutrients. Using the same method as Tam et al. [5], we estimate the diffusion coefficient of glucose in agar to be $D_s = 4.01 \times 10^{-2}\,\mathrm{mm}^2 \cdot \mathrm{min}^{-1}$ [58, 59]. For the mass transfer coefficient of nutrients within the biofilm, we cite Vicente et al. [61], who estimate the mass transfer coefficient of glucose in a yeast (*S. cerevisiae*) floc to be $Q = 2.92 \times 10^{-3}\,\mathrm{mm} \cdot \mathrm{min}^{-1}$. Stewart [60] conducted a review of experimental measurements of diffusivity in biofilms of different bacterial and fungal species. They found that the average effective diffusivity of glucose in a microbial biofilm was $0.24D_{aq}$, where $D_{aq} = 4.04 \times 10^{-2}\,\mathrm{mm}^2 \cdot \mathrm{min}^{-1}$ is the diffusivity of glucose in water [59]. Thus, a suitable estimate is $D_b = 9.70 \times 10^{-3}\,\mathrm{mm}^2 \cdot \mathrm{min}^{-1}$. This is of the same order of magnitude as an estimate for colony of *S. cerevisiae*, which Vicente et al. [61] give as $D_b = 6.6 \times 10^{-3}\,\mathrm{mm}^2 \cdot \mathrm{min}^{-1}$.

The cell production rate ψ_n and nutrient consumption rate η are chosen to minimise the sum of squared differences between numerical solutions and the experimental data. We found that the combination of $\psi_n = 12.1\,\mathrm{mm}^2 \cdot \mathrm{g}^{-1} \cdot \mathrm{min}^{-1}$ and $\eta = 3.7 \times 10^{-3}\,\mathrm{min}^{-1}$ produced a local minimum in the error, and therefore we adopted these as our parameter estimates. At the same time, we estimate the ECM production rate ψ_m using the experimental observation that extracellular material occupies approximately 10% of mature *S. cerevisiae* mats by volume, and therefore assume $\Psi_m = 1/9$. This is now sufficient to determine representative values for all of the dimensionless parameters in Table 3.1.

B Numerical method

As mentioned in §4.1, before solving the 1D radial model numerically, we apply the change of variables (4.1) to map both the biofilm and unoccupied Petri dish domains to the unit interval. The governing equations to solve then become

$$\frac{\partial h}{\partial t} - \frac{\xi}{S}\frac{\mathrm{d}S}{\mathrm{d}t}\frac{\partial h}{\partial \xi} + \frac{1}{S\xi}\frac{\partial}{\partial \xi}\left(\xi u_r h\right) = \left(1 + \Psi_m\right)\bar{\phi}_n g_b h, \tag{B.1a}$$

$$\frac{\partial \bar{\phi}_n}{\partial t} + \frac{1}{S}\left(u_r - \xi\frac{\mathrm{d}S}{\mathrm{d}t}\right)\frac{\partial \bar{\phi}_n}{\partial \xi} = \bar{\phi}_n\left[g_b - \Psi_d - \left(1 + \Psi_m\right)\bar{\phi}_n g_b\right], \tag{B.1b}$$

$$\frac{\partial g_s}{\partial t} - \frac{\xi}{S}\frac{\mathrm{d}S}{\mathrm{d}t}\frac{\partial g_s}{\partial \xi} = \frac{D}{S^2\xi}\frac{\partial}{\partial \xi}\left(\xi\frac{\partial g_s}{\partial \xi}\right) - DQ_s\left(g_s - g_b\right), \tag{B.1c}$$

$$\begin{aligned}\frac{\partial g_{so}}{\partial t} + \frac{1 - \xi_o}{R - S}\frac{\mathrm{d}S}{\mathrm{d}t}\frac{\partial g_{so}}{\partial \xi_o} &= \frac{D}{(R-S)^2}\frac{\partial^2 g_{so}}{\partial \xi_o^2} \\ &+ \frac{D}{S(R-S) + \xi_o(R-S)^2}\frac{\partial g_{so}}{\partial \xi_o},\end{aligned} \tag{B.1d}$$

$$\mathrm{Pe}\left\{h\frac{\partial g_b}{\partial t}-h\frac{\xi}{S}\frac{\mathrm{d}S}{\mathrm{d}t}\frac{\partial g_b}{\partial \xi}+\frac{1}{S\xi}\frac{\partial}{\partial \xi}\left[\xi u_r\left(1-\bar{\phi}_n\right)g_b h\right]\right\}= \frac{1}{S^2\xi}\frac{\partial}{\partial \xi}\left(\xi h\frac{\partial g_b}{\partial \xi}\right)+Q_b\left(g_s-g_b\right)-\Upsilon\bar{\phi}_n g_b h, \tag{B.1e}$$

$$\frac{4}{S}\frac{\partial}{\partial \xi}\left[\frac{h}{\xi}\frac{\partial}{\partial \xi}\left(\xi u_r\right)\right]-\frac{2u_r}{S\xi}\frac{\partial h}{\partial \xi}=2\left(1+\Psi_m\right)\frac{\partial}{\partial \xi}\left(\bar{\phi}_n g_b h\right) -\frac{\gamma^* h}{S^2}\frac{\partial}{\partial \xi}\left[\frac{1}{\xi}\frac{\partial}{\partial \xi}\left(\xi\frac{\partial h}{\partial \xi}\right)\right], \tag{B.1f}$$

$$\frac{\mathrm{d}S}{\mathrm{d}t}=u_r\left(1,t\right), \tag{B.1g}$$

where g_{s_o} denotes the nutrient concentration in the region of the substratum that is not occupied by the biofilm. Under the change of variables (4.1), the initial conditions are

$$S(0)=1,\quad h(\xi,0)=H_0\left(1-\xi^2\right),\quad \bar{\phi}_n(\xi,0)=1, \quad g_s(\xi,0)=g_{s_o}(\xi_o,0)=1,\quad g_b(\xi,0)=0, \tag{B.2}$$

the boundary conditions become

$$\left.\frac{\partial h}{\partial \xi}\right|_{(0,t)}=0,\quad \left.\frac{\partial \bar{\phi}_n}{\partial \xi}\right|_{(0,t)}=0,\quad \left.\frac{\partial g_s}{\partial \xi}\right|_{(0,t)}=0,\quad \left.\frac{\partial g_b}{\partial \xi}\right|_{(0,t)}=0,\quad u_r(0,t)=0, \quad \left.\frac{\partial g_{s_o}}{\partial \xi_o}\right|_{(1,t)}=0,\quad \left.\frac{\partial g_b}{\partial \xi}\right|_{(1,t)}=0, \tag{B.3}$$

$$\left.\frac{4}{S}\frac{\partial u_r}{\partial \xi}\right|_{(1,t)}+\frac{2u_r(1,t)}{S}=2\left(1+\Psi_m\right)\bar{\phi}_n(1,t)g_b(1,t)-\frac{\gamma^*}{S^2}\left.\frac{\partial}{\partial \xi}\left(\xi\frac{\partial h}{\partial \xi}\right)\right|_{(1,t)},$$

and we must also satisfy the continuity conditions

$$g_s\left(1,t\right)=g_{s_o}\left(0,t\right),\quad \left.\frac{1}{S}\frac{\partial g_s}{\partial \xi}\right|_{(1,t)}=\left.\frac{1}{R-S}\frac{\partial g_{s_o}}{\partial \xi_o}\right|_{(0,t)}. \tag{B.4}$$

Producing a numerical solution to the 1D axisymmetric extensional flow model then requires solving the system (B.1), subject to (B.2)–(B.4), on $\xi\in[0,1]$, $\xi_o\in[0,1]$, and $t\in[0,T]$.

We solve the model on equispaced grids in time and space. For the time domain, we denote the discrete grid points by $t^k=(k-1)\Delta t$, for $k=1,\ldots,N_t$, where $\Delta t=T/(N_t-1)$. For both the biofilm and outer Petri dish domains, we define $\xi_j=(j-1)\Delta\xi$ and $\xi_{oj}=(j-1)\Delta\xi_o$ for $j=1,\ldots,N_\xi$, where $\Delta\xi=1/(N_\xi-1)$ and $\Delta\xi_o=1/(N_{\xi_o}-1)$, to represent the discrete grid points. After prescribing the initial conditions, we first solve (B.1f) to determine the initial fluid velocity. Following this, at each time step we solve the

equations in the order listed in (B.1), until the final time $t^{N_t} = T$ is reached.

We discretise the governing equations using a finite difference Crank–Nicolson scheme. Where necessary, we linearise nonlinear terms using data from the previous time step. In the equations for h and u_r, we first expand relevant derivative terms using the product rule before discretising the equations. At the interior grid points $j = 2, \dots N_\xi - 1$, the numerical scheme then reads

$$\begin{aligned}
&\frac{h_j^k - h_j^{k-1}}{\Delta t} + \left(\frac{u_{rj}^{k-1} - \xi_j u_{rN_\xi}^{k-1}}{S^{k-1}}\right) \frac{h_{j+1}^{k-1/2} - h_{j-1}^{k-1/2}}{2\Delta\xi} \\
&+ \left(\frac{u_{rj+1}^{k-1} - u_{rj-1}^{k-1}}{2S^{k-1}\Delta\xi} + \frac{u_{rj}^{k-1}}{S^{k-1}\xi_j}\right) h_j^{k-1/2} = (1 + \Psi_m)\, \bar{\phi}_{nj}^{\,k-1} g_{bj}^{\,k-1} h_j^{k-1/2},
\end{aligned} \tag{B.5a}$$

$$\begin{aligned}
&\frac{\bar{\phi}_{nj}^{\,k} - \bar{\phi}_{nj}^{\,k-1}}{\Delta t} + \left(\frac{u_{rj}^{k-1} - \xi_j u_{rN_\xi}^{k-1}}{S^{k-1}}\right) \frac{\bar{\phi}_{nj+1}^{\,k-1/2} - \bar{\phi}_{nj-1}^{\,k-1/2}}{2\Delta\xi} \\
&= \bar{\phi}_{nj}^{\,k-1/2} \left[g_{bj}^{\,k-1} - \Psi_d - (1 + \Psi_m)\, \bar{\phi}_{nj}^{\,k-1} g_{bj}^{\,k-1}\right],
\end{aligned} \tag{B.5b}$$

$$\begin{aligned}
&\frac{g_{sj}^{\,k} - g_{sj}^{\,k-1}}{\Delta t} - \left(\frac{\xi_j u_{rN_\xi}^{k-1}}{S^{k-1}}\right) \frac{g_{sj+1}^{\,k-1/2} - g_{sj-1}^{\,k-1/2}}{2\Delta\xi} \\
&= \frac{D}{\left(S^{k-1}\right)^2 \xi_j} \left[\frac{(\xi_{j+1} + \xi_j)\left(g_{sj+1}^{\,k-1/2} - g_{sj}^{\,k-1/2}\right)}{2\left(\Delta\xi\right)^2}\right] \\
&- \frac{D}{\left(S^{k-1}\right)^2 \xi_j} \left[\frac{(\xi_j + \xi_{j-1})\left(g_{sj}^{\,k-1/2} - g_{sj-1}^{\,k-1/2}\right)}{2\left(\Delta\xi\right)^2}\right] \\
&- DQ_s \left(g_{sj}^{\,k-1/2} - g_{bj}^{\,k-1}\right),
\end{aligned} \tag{B.5c}$$

$$\begin{aligned}
&\frac{g_{soj}^{\,k} - g_{soj}^{\,k-1}}{\Delta t} + \left(\frac{1 - \xi_{oj}}{R - S^{k-1}} u_{rN_\xi}^{k-1}\right) \frac{g_{soj+1}^{\,k-1/2} - g_{soj-1}^{\,k-1/2}}{2\Delta\xi_o} \\
&= \frac{D}{\left(R - S^{k-1}\right)^2} \frac{g_{soj+1}^{\,k-1/2} - 2g_{soj}^{\,k-1/2} + g_{soj-1}^{\,k-1/2}}{\left(\Delta\xi_o\right)^2} \\
&+ \left[\frac{D}{S^{k-1}\left(R - S^{k-1}\right) + \xi_{oj}\left(R - S^{k-1}\right)^2}\right] \frac{g_{soj+1}^{\,k-1/2} - g_{soj-1}^{\,k-1/2}}{2\Delta\xi},
\end{aligned} \tag{B.5d}$$

$$
\begin{aligned}
&\mathrm{Pe}h_j^{k-1}\frac{g_{bj}^{k}-g_{bj}^{k-1}}{\Delta t}-\left(\frac{\mathrm{Pe}h_j^{k-1}\xi_j u_{rN_\xi}^{k-1}}{S^{k-1}}\right)\frac{g_{bj+1}^{k-1/2}-g_{bj-1}^{k-1/2}}{2\Delta\xi}\\
&+\frac{\mathrm{Pe}}{S^{k-1}\xi_j}\frac{\left[\xi u_r\left(1-\bar{\phi}_n\right)h\right]_{j+1}^{k-1}g_{bj+1}^{k-1/2}-\left[\xi u_r\left(1-\bar{\phi}_n\right)h\right]_{j-1}^{k-1}g_{bj-1}^{k-1/2}}{2\Delta\xi}\\
&=\frac{1}{\left(S^{k-1}\right)^2\xi_j}\left[\frac{\left(\xi_{j+1}h_{j+1}^{k-1}+\xi_j h_j^{k-1}\right)\left(g_{bj+1}^{k-1/2}-g_{bj}^{k-1/2}\right)}{2\left(\Delta\xi\right)^2}\right]\\
&-\frac{1}{\left(S^{k-1}\right)^2\xi_j}\left[\frac{\left(\xi_j h_j^{k-1}+\xi_{j-1}h_{j-1}^{k-1}\right)\left(g_{bj}^{k-1/2}-g_{bj-1}^{k-1/2}\right)}{2\left(\Delta\xi\right)^2}\right]\\
&+Q_b\left(g_{sj}^{k-1}-g_{bj}^{k-1/2}\right)-\Upsilon\bar{\phi}_{nj}^{k-1}g_{bj}^{k-1/2}h_j^{k-1},
\end{aligned}
\tag{B.5e}
$$

$$
\begin{aligned}
&\left(\frac{4h_j^k}{S^{k-1}}\right)\frac{u_{rj+1}^{k}-2u_{rj}^{k}+u_{rj-1}^{k}}{\left(\Delta\xi\right)^2}\\
&+\frac{4}{S^{k-1}}\left(\frac{h_{j+1}^k-h_{j-1}^k}{2\Delta\xi}+\frac{h_j^k}{\xi_j}\right)\frac{u_{rj+1}^{k}-u_{rj-1}^{k}}{2\Delta\xi}\\
&+\frac{2}{S^{k-1}\xi_j}\left(\frac{h_{j+1}^k-h_{j-1}^k}{2\Delta\xi}-\frac{2h_j^k}{\xi_j}\right)u_{rj}^{k}\\
&=2\left(1+\Psi_m\right)\left[\frac{\left(\bar{\phi}_n g_b h\right)_{j+1}^{k}-\left(\bar{\phi}_n g_b h\right)_{j-1}^{k}}{2\Delta\xi}\right]-\Gamma_j^k,
\end{aligned}
\tag{B.5f}
$$

$$
\frac{S^k-S^{k-1}}{\Delta t}=u_{rN_\xi}^{k-1/2},
\tag{B.5g}
$$

where we approximate terms at the half time points using

$$
h_j^{k-1/2}=\frac{h_j^k+h_j^{k-1}}{2},
\tag{B.6}
$$

and so on. In (B.5f), Γ_j^k denotes the discretised surface tension term, which we discuss in detail later. In conjunction with appropriate boundary schemes, each equation in (B.5) describes a linear system to solve for the variables at $t=t^k$.

We need to take particular care at domain boundaries to prevent spurious oscillations appearing in the solution. At $\xi=0$ and $\xi_o=0$, we obtained the best results by substituting the boundary conditions into discretised forms of the equations (B.1c) and (B.1e), using one-sided differences for first derivative terms and introducing fictitious grid points for second derivative terms. For (B.1a), (B.1b), (B.1d) and (B.1f) we apply the relevant boundary conditions explicitly. Although the equations (B.1c) and (B.1e) are singular at $\xi=0$, we can use L'Hôpital's rule to evaluate the relevant terms as $\xi\to 0$. The boundary

schemes are then

$$\frac{-3h_1^k + 4h_2^k - h_3^k}{2\Delta\xi} = 0, \tag{B.7a}$$

$$\frac{-3{\phi_{n1}}^k + 4{\phi_{n2}}^k - {\phi_{n3}}^k}{2\Delta\xi} = 0, \tag{B.7b}$$

$$\frac{{g_{s1}}^k - {g_{s1}}^{k-1}}{\Delta t} = \frac{4D}{\left(S^{k-1}\right)^2}\frac{{g_{s2}}^{k-1/2} - {g_{s1}}^{k-1/2}}{\left(\Delta\xi\right)^2} - DQ_s\left({g_{s1}}^{k-1/2} - {g_{b1}}^{k-1}\right), \tag{B.7c}$$

$${g_{so1}}^k = a, \tag{B.7d}$$

$$\begin{aligned} &\mathrm{Pe}h_1^{k-1}\frac{{g_{b1}}^k - {g_{b1}}^{k-1}}{\Delta t} \\ &+\frac{\mathrm{Pe}\left(1-{\bar{\phi}_{n1}}^{k-1}\right)h_1^{k-1}\left(-3{u_{r1}}^{k-1} + 4{u_{r2}}^{k-1} - {u_{r3}}^{k-1}\right)}{S^{k-1}\Delta\xi}{g_{b1}}^{k-1/2} \\ &= \frac{4h_1^{k-1}}{\left(S^{k-1}\right)^2}\frac{{g_{b2}}^{k-1/2} - {g_{b1}}^{k-1/2}}{\left(\Delta\xi\right)^2} + Q_b\left({g_{b1}}^{k-1/2} - {g_{s1}}^k\right) \\ &-\Upsilon{\bar{\phi}_{n1}}^{k-1}{g_{b1}}^{k-1/2}h_1^{k-1}, \end{aligned} \tag{B.7e}$$

$${u_{r1}}^k = 0, \tag{B.7f}$$

where a is the value of $g_s(S(t),t)$. At $\xi = 1$ and $\xi_o = 1$, we solve the equations (B.1a), (B.1b) and (B.1d) directly, again using one-sided differences for first derivatives and introducing fictitious grid points for second derivatives. We apply the Dirichlet condition for g_s, and as (B.1e) is singular as $h \to 0$, we impose the boundary condition for g_b directly using a one-sided difference. We also obtained best results by apply the zero radial stress condition directly at $\xi = 1$. The boundary schemes are then

$$\begin{aligned} &\frac{h_{N_\xi}^k - h_{N_\xi}^{k-1}}{\Delta t} + \left(\frac{3{u_r}_{N_\xi}^{k-1} - 4{u_r}_{N_\xi-1}^{k-1} + {u_r}_{N_\xi-2}^{k-1}}{2S^{k-1}\Delta\xi} + \frac{{u_r}_{N_\xi}^{k-1}}{S^{k-1}}\right)h_{N_\xi}^{k-1/2} \\ &= \left(1+\Psi_m\right){\bar{\phi}_{n}}_{N_\xi}^{k-1}{g_b}_{N_\xi}^{k-1}h_{N_\xi}^{k-1/2}, \end{aligned} \tag{B.8a}$$

$$\frac{{\bar{\phi}_{n}}_{N_\xi}^{k} - {\bar{\phi}_{n}}_{N_\xi}^{k-1}}{\Delta t} = {\bar{\phi}_{n}}_{N_\xi}^{k-1/2}\left[{g_b}_{N_\xi}^{k-1} - \Psi_d - \left(1+\Psi_m\right){\bar{\phi}_{n}}_{N_\xi}^{k-1}{g_b}_{N_\xi}^{k-1}\right], \tag{B.8b}$$

$${g_s}_{N_\xi}^k = a, \tag{B.8c}$$

$$\frac{{g_{so}}_{N_\xi}^{k} - {g_{so}}_{N_\xi}^{k-1}}{\Delta t} = \frac{D}{\left(R-S\right)^2}\frac{2{g_{so}}_{N_\xi-1}^{k-1/2} - 2{g_{so}}_{N_\xi}^{k-1/2}}{\left(\Delta\xi\right)^2}, \tag{B.8d}$$

$$\frac{3{g_b}_{N_\xi}^k - 4{g_b}_{N_\xi-1}^k + {g_b}_{N_\xi-2}^k}{2\Delta\xi} = 0, \tag{B.8e}$$

$$\frac{2}{S^{k-1}}\left(\frac{3u_r{}^k_{N_\xi}-4u_r{}^k_{N_\xi-1}+u_r{}^k_{N_\xi-2}}{\Delta\xi}+u_r{}^k_{N_\xi}\right) = 2\left(1+\Psi_m\right)\bar{\phi}_n{}^k_{N_\xi} g_b{}^k_{N_\xi}-\Gamma^k_{N_\xi}, \tag{B.8f}$$

where $\Gamma^k_{N_\xi}$ is the contribution of surface tension to the no radial stress boundary condition in (B.3).

For the surface tension terms, we expand the derivative terms and write

$$\Gamma^k_j = \frac{h^k_j}{(S^k)^2}\left[\frac{\partial^3 h}{\partial\xi^3}+\frac{1}{\xi}\frac{\partial^2 h}{\partial\xi^2}-\frac{1}{\xi^2}\frac{\partial h}{\partial\xi}\right]^k_j, \quad \text{for} \quad j=2,\dots N_\xi-1, \tag{B.9a}$$

$$\Gamma^k_{N_\xi} = \frac{1}{(S^k)^2}\left[\xi\frac{\partial^2 h}{\partial\xi^2}+\frac{\partial h}{\partial\xi}\right]^k_{N_\xi}. \tag{B.9b}$$

To compute the first spatial derivative of h, we use standard sixth-order accurate finite difference formulae. We then use the same scheme to compute the higher derivatives sequentially, that is

$$\frac{\partial^2 h}{\partial\xi^2}=\frac{\partial}{\partial\xi}\left(\frac{\partial h}{\partial\xi}\right), \quad \text{and} \quad \frac{\partial^3 h}{\partial\xi^3}=\frac{\partial}{\partial\xi}\left[\frac{\partial}{\partial\xi}\left(\frac{\partial h}{\partial\xi}\right)\right], \tag{B.10}$$

where we represent differentiation operators with the finite difference scheme. When $\gamma^*\neq 0$, we required a larger number of time steps to produce solutions without spurious oscillations in the surface tension term. Therefore, all solutions involving surface tension were computed with $N_\xi = 1001$ and $N_t = 2000001$. The convergence analysis in §B.1 suggests that this will produce solutions that are accurate to approximately 0.4% relative error.

A feature of our model is that finding the nutrient concentration in the substratum requires solving both (B.1c) and (B.1d), and ensuring that the continuity conditions (B.4) are satisfied. To do this, we first solve (B.1c) and (B.1d), in both cases assuming the Dirichlet conditions $g_s(1,t^k)=g_{so}(0,t^k)=a$, with $a=g_s(1,t^{k-1})$, as an initial guess. To ensure continuity of the derivative, we define and compute

$$f(a)=\frac{1}{R-S}\frac{\partial g_{s_o}}{\partial\xi_o}\bigg|_{(0,t)}-\frac{1}{S}\frac{\partial g_s}{\partial\xi}\bigg|_{(1,t)}, \tag{B.11}$$

for the initial guess of a, with both derivatives in (B.11) approximated using second-order one-sided finite differences. We then use Newton's method to drive $f(a)$ to zero, where we approximate the required derivative numerically using

$$\frac{\mathrm{d}f}{\mathrm{d}a}=\frac{f(a+\delta)-f(a)}{\delta}, \tag{B.12}$$

for $\delta = 1 \times 10^{-6}$, and iterate until a is accurate to 1×10^{-6}. This procedure allows us to solve for g_s over the entire Petri dish domain at each time step.

B.1 Convergence of the numerical method

The numerical solutions in §4.1 were computed using $N_\xi = 8001$ grid points and $N_t = 160001$ time steps, giving $\Delta\xi = 1.25 \times 10^{-4}$ and $\Delta t \approx 1 \times 10^{-4}$. To verify that this is sufficient to produce a converged solution, we repeated the computation using a range of grid spacings and time step sizes. In each case, we computed the contact line position at $t = 15.9$, which yielded the results shown in Figure B.1. The numerical scheme exhibits

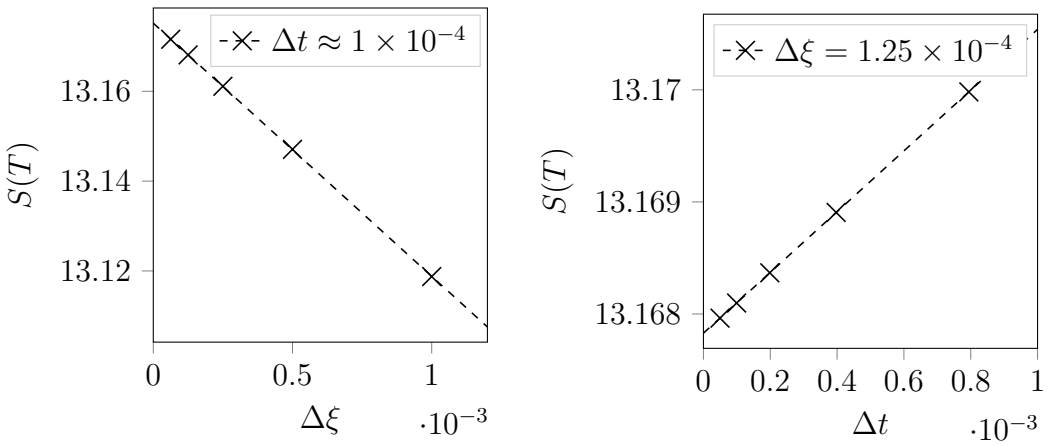

(a) Numerical results for $\Delta t \approx 1 \times 10^{-4}$, and $\Delta\xi \to 0$.

(b) Numerical results for $\Delta\xi = 1.25 \times 10^{-4}$, and $\Delta t \to 0$.

Figure B.1: Convergence of the numerical scheme for the axisymmetric extensional flow model. At each data point, we plot the biofilm radius attained at the experimental time $t = T$.

linear convergence with both grid spacing and time step size. By fitting a straight line to the data in Figure B.1 and extrapolating, we can estimate the numerical contact line position in the zero grid spacing and time step limit. Doing so, we find that when $\Delta t \approx 1 \times 10^{-4}$, the estimated contact line position as $\Delta\xi \to 0$ is $S(T) = 13.1752$. When $\Delta\xi = 1.25 \times 10^{-4}$, the estimated contact line position as $\Delta t \to 0$ is $S(T) = 13.1678$. As these are within approximately 0.05% of each other and the numerical value for the chosen grid spacing and time step size, $S(T) = 13.1681$, we conclude that our numerical solution is sufficiently converged.

C Statements

C.1 Ethics

No ethical approval was required for this research.

C.2 Data, code, and materials

Data and code for this research are available at The University of Adelaide's Figshare repository, at https://doi.org/10.25909/5c93294133642.

C.3 Competing interests

The authors declare no competing interests.

C.4 Author contributions

All authors designed the research. A. T. performed the mathematical modelling and numerical computation, with assistance from B. J. B., J. E. F. G., and S. B., and wrote the manuscript. E. L. T., J. M. G., and J. F. S. performed the mat formation experiments under supervision of V. J., and collected the data. All authors provided comments and guidance on the manuscript.